

RESEARCH ARTICLE

miR-31-mediated local translation at the mitotic spindle is important for early development

Carolyn M. Remsburg¹, Kalin D. Konrad^{1,2,*}, Michael D. Testa^{1,*}, Nadezda Stepicheva^{1,3}, Kelvin Lee^{4,5}, Leila H. Choe^{4,5}, Shawn Polson⁶, Jaysheel Bhavsar⁷, Hongzhan Huang⁷ and Jia L. Song^{1,‡}

ABSTRACT

miR-31 is a highly conserved microRNA that plays crucial roles in cell proliferation, migration and differentiation. We discovered that miR-31 and some of its validated targets are enriched on the mitotic spindle of the dividing sea urchin embryo and mammalian cells. Using the sea urchin embryo, we found that miR-31 inhibition led to developmental delay correlated with increased cytoskeletal and chromosomal defects. We identified miR-31 to directly suppress several actin remodeling transcripts, including β -actin, Gelsolin, Rab35 and Fascin. De novo translation of Fascin occurs at the mitotic spindle of sea urchin embryos and mammalian cells. Importantly, miR-31 inhibition leads to a significant a increase of newly translated Fascin at the spindle of dividing sea urchin embryos. Forced ectopic localization of Fascin transcripts to the cell membrane and translation led to significant developmental and chromosomal segregation defects, highlighting the importance of the regulation of local translation by miR-31 at the mitotic spindle to ensure proper cell division. Furthermore, miR-31-mediated post-transcriptional regulation at the mitotic spindle may be an evolutionarily conserved regulatory paradigm of mitosis.

KEY WORDS: Sea urchin, Cleavage stage, Cytoskeletal elements, Cell division

INTRODUCTION

Mitosis is a fundamental process that results in the faithful segregation of chromosomes to each resulting daughter cell (Batty and Gerlich, 2019). Misregulation of mitosis can lead to cell death, arrest or DNA damage (Lanni and Jacks, 1998; Orth et al., 2012). Faithful segregation of chromosomes into daughter cells is mediated by the mitotic spindle, which is composed primarily of microtubules (McIntosh, 2016) and associated proteins. The mitotic spindle is regulated by a complex set of RNAs, microtubule motors, polymerizing factors, as well as by actin (Kita et al., 2019).

¹Department of Biological Sciences, University of Delaware, Newark, DE 19716, USA. ²Department of Neurology, Columbia University, New York, NY 10032, USA. ³Department of Ophthalmology, University of Pittsburgh, Pittsburgh, PA 15224, USA. ⁴Department of Chemical and Biomolecular Engineering, University of Delaware, Newark, DE 19716, USA. ⁵National Institute for Innovation in Manufacturing Biopharmaceuticals, Newark, DE 19716, USA. ⁶Department of Computer and Informational Sciences; Plant & Soil Sciences; Biological Sciences, CBCB Bioinformatics Core Facility; Bioinformatics, Healthcare Informatics, and Data Science Network of Delaware, University of Delaware, Newark, DE 19716, USA. ⁷Department of Computer and Informational Sciences, University of Delaware, DE 19716, USA.

© C.M.R., 0000-0002-8977-9334; K.D.K., 0009-0000-5405-7967; K.L., 0000-0003-0908-2981; S.P., 0000-0002-3398-6932; J.L.S., 0000-0002-5664-1136

Handling Editor: Cassandra Extavour Received 15 December 2023; Accepted 17 July 2024 To date, post-transcriptional regulation mediated by microRNAs (miRNAs) at the mitotic spindle has not been examined.

The long-held belief has been that translation is generally repressed during mitosis. However, these studies were often performed using cell-cycle synchronization techniques that rely on microtubule disruption or inhibition of DNA synthesis, which stress the cell and lead to global translational repression (Tanenbaum et al., 2015). In recent studies, it has been shown that the magnitude of this repression is considerably less than previously thought. For example, using CDK inhibition leads to only a 35% reduction in translation, whereas temperature-sensitive mutants of cdc-10, cdc-25 and nda3, and fluorescence activated cell sorting of non-synchronized cells reveal no significant cell cycle-dependent differences in translation (Tanenbaum et al., 2015; Stonyte et al., 2018). Additional data suggest that mitosis-related proteins, such as cohesins, cyclins and mitotic spindle components are more likely to be translated during mitosis (Imami et al., 2018). These new data indicate that translation is not globally inhibited during mitosis; instead, specific proteins are being translated during this time.

Evidence of local translation during mitosis has also emerged, as translational initiation and elongation factors, ribosomal proteins, and various RNA species have been observed on the mitotic spindle (Chassé et al., 2016; Hassine et al., 2020; Pascual et al., 2021; Fernandez-Nicolas et al., 2022). Biochemical analyses have revealed that a complex pool of mRNAs, lncRNAs and miRNAs associate with the mitotic spindle (Hassine et al., 2020; Blower et al., 2007). Many of these spindle-associated mRNAs encode proteins that regulate various aspects of mitosis (Blower et al., 2007). We have recently identified several mRNAs encoding proteins that regulate mitosis and are localized to the mitotic spindle (Remsburg et al., 2023). Disruption of the localization of one of these transcripts, AuroraB, results in early embryonic developmental delay and lethality (Remsburg et al., 2023). Furthermore, mRNAs, RNAbinding proteins, ribosomal and translational regulators, and RNAprocessing proteins are found in the midbody (Farmer et al., 2023; Park et al., 2023; Skop et al., 2004; Capalbo et al., 2019; Addi et al., 2020; Peterman and Prekeris, 2019). Stored mRNAs in the midbodies can undergo active translation in late telophase in pre-abscission daughter cells (Park et al., 2023), and can be internalized by other cells to regulate cell proliferation and differentiation (Addi et al., 2020; Peterman and Prekeris, 2019). These studies strongly suggest that subcellular localization of transcripts and their translation at the mitotic spindle may play an important role in the progression of mitosis and early development.

miR-31 is a highly conserved microRNA that has been examined in myogenesis, bone homeostasis, skeletogenesis and cancer (Su et al., 2020; Stepicheva and Song, 2015; Crist et al., 2012; Cekaite et al., 2012; Lv et al., 2017; Mizoguchi et al., 2013; Ge et al., 2017; Tian et al., 2017; Zheng et al., 2021). We have previously identified miR-31 as suppressing several transcription factors and signaling

^{*}These authors contributed equally to this work

[‡]Author for correspondence (jsong@udel.edu)

pathway components to modulate sea urchin skeletogenesis (Stepicheva and Song, 2015; Sampilo et al., 2021).

Post-transcriptional regulation by miRNAs occurs in most protein-coding genes and may be a mechanism for regulating local translation at the mitotic spindle. The early cleavage stage of development in metazoans is characterized by a series of rapid cell divisions (Siefert et al., 2015), during which efficient and rapid protein regulation is important. In examining the role miR-31 plays in development (Stepicheva and Song, 2015), we discovered that miR-31 has a cell cycle-dependent subcellular localization to the perinuclear region and the mitotic spindle (Figs 1 and 3). Using highthroughput approaches, we use the sea urchin embryo to identify the regulatory role of miR-31 during mitosis and validate several miR-31 targets, including β -actin, Gelsolin, Rab35 and Fascin (Fig. 2). We found Fascin mRNA to be actively translated at the spindle of sea urchin embryos and mammalian cells. Furthermore, inhibition of miR-31 leads to significantly increased de novo Fascin protein synthesis at the mitotic spindle of dividing sea urchin embryos (Figs 4 and 5). Forced ectopic translation of Fascin mRNA at the cell membrane results in developmental delay and chromosomal defects, leading to the hypothesis that miR-31 mediates local translation of cytoskeletal modulating mRNAs, such as Fascin and Rab35, at the mitotic spindle to fine-tune mitosis (Figs 6 and 7). Fascin protein cross-links F-actin into linear bundles, and interacts with and promotes microtubule polymerization (Villari et al., 2015; Jayo and Parsons, 2010); Rab35 is a small GTPase that directly interacts with Fascin protein and regulates actin polymerization (Remsburg et al., 2021; Klinkert et al., 2016). We propose that regulated local translation of Fascin and Rab35 at the mitotic spindle may allow rapid polymerization of the cytoskeleton that is needed to mediate the timely segregation of chromosomes. This is the first study demonstrating that miRNA-mediated post-transcriptional regulation of cytoskeletal elements is necessary for development. Importantly, this regulation of mitosis may be evolutionarily conserved.

RESULTS

$\operatorname{miR-31}$ has a dynamic localization that correlates to the cell cycle

In examining the role of miR-31 in development, we discovered that miR-31 has a cell cycle-dependent distribution (Fig. 1A), miR-31 is enriched on the mitotic spindle in dividing cells and in the perinuclear region of non-dividing cells of sea urchin embryos. The association of miR-31 with the mitotic spindle continues to at least the early blastula stage (Fig. 1A). Based on the structure of the chromosomes and microtubules, we took images and analyzed the localization and enrichment of miR-31 throughout stages of the cell cycle (Fig. 1B). During interphase, miR-31 is enriched in the perinuclear region. miR-31 levels are the highest in metaphase and anaphase, where it is enriched in the spindle midzone. In telophase, miR-31 is still enriched in the midzone but its level is similar to that in interphase. miR-31 appears to be enriched in the presumptive midbody in 73% and 62.5% of the early and late telophase blastomeres, respectively. This enrichment of miR-31 at the spindle midzone is specific, as we do not observe miR-124 localizing to the mitotic spindle in early cleavage stage embryos (Fig. 1A).

miR-31-inhibited embryos are developmentally delayed, exhibit chromosomal segregation defects, and have increased microtubules and F-actin

To test the function of miR-31, we injected a miR-31 locked-nucleic acid (LNA) inhibitor into newly fertilized eggs, using a miR-124 LNA inhibitor as a control for LNA toxicity. miR-124 is not

expressed until 12 h post-fertilization (hpf) (Konrad et al., 2023) and embryos injected with miR-124 LNA inhibitor exhibit normal early cleavage stage development, similar to control embryos injected with a dextran (Fig. 1Di). Using fluorescence *in situ* hybridization (FISH) to assess the efficacy of the miR-31 inhibitor, we observe a significant decrease in detectable miR-31 in miR-31 inhibitor-injected embryos, indicating that the majority of endogenous miR-31 is likely to be bound to the miR-31 inhibitor and not available for miR-31 RNA probe binding (Fig. 1Dii).

We observe that inhibition of miR-31 results in a significant delay or arrest in embryonic development or embryonic lethality compared with the control miR-124 inhibitor-injected embryos (Fig. 1Diii). As early as 2 hpf, we observed significant differences between control and miR-31 inhibitor-injected embryos in terms of the percentage of embryos that have advanced to the two-cell stage. This significant difference in development continues to 6 hpf, where 66% and 14% of control and miR-31 inhibitor-injected embryos develop to the 32-cell stage, respectively (Fig. 1Diii). This difference in developmental delay persists to the blastula stage, as 90% and 70% of the control and miR-31 inhibitor-injected embryos survived to the blastula stage, respectively (Fig. 1Diii).

As miR-31 inhibition leads to early developmental delay and/or arrest at a time when the embryos rapidly divide, we investigated chromosomal integrity in these early cleavage stage embryos. In dividing blastomeres, we observed that ~25% of blastomeres exhibit chromosomal defects, including uncondensed chromosomes, lagging chromosomes or DNA bridging (Fig. 1E). These results suggest that miR-31 inhibition leads to chromosomal segregation defects. In addition, we did not observe a difference between the proportion of blastomeres in a particular mitotic phase between control and miR-31-inhibited embryos, suggesting that miR-31 does not seem to inhibit a particular phase of mitosis (Fig. S1).

As proper chromosomal segregation is dependent upon formation of the mitotic spindle, we examined the structure of the cytoskeleton. miR-31 inhibition results in significantly increased microtubules, including interpolar and kinetochore microtubules during anaphase (Fig. 1F), as well as significantly increased filamentous actin (F-actin) in miR-31-inhibited blastomeres in anaphase compared with the control-injected embryos (Fig. 1G). Results indicate that total levels of monomeric tubulin and actin in control and miR-31-inhibited embryos did not significantly differ, suggesting that miR-31 may regulate the polymerization of these cytoskeletal proteins (Fig. 1Fiii,Giii).

Identification of miR-31 targets reveals targets that encode regulators of cytoskeletal dynamics

To determine potential miR-31 targets, we took two different highthroughput approaches. We injected zygotes with either a scramble control or miR-31 inhibitor and subjected to two four-plex isobaric tagging methods for quantification of their proteomes (Table S1). Proteins that had increased levels upon miR-31 inhibition compared with the control were analyzed bioinformatically. We also injected biotinylated miR-31 mimic into the zygotes, in which the miR-31 would become incorporated into the RNA-induced silencing complex (RISC) and bind to endogenous miR-31 targets (Table S2). Embryonic lysates were passed over a streptavidin bead-coated column, and the bound RNA transcripts were eluted and identified using RNA sequencing. From both approaches, we identified a list of potential miR-31 targets and focused on transcripts encoding proteins that regulate cytoskeletal dynamics that may impact cell division. As these approaches often have high background that may not be specific, we validated these targets by demonstrating that miR-31 directly

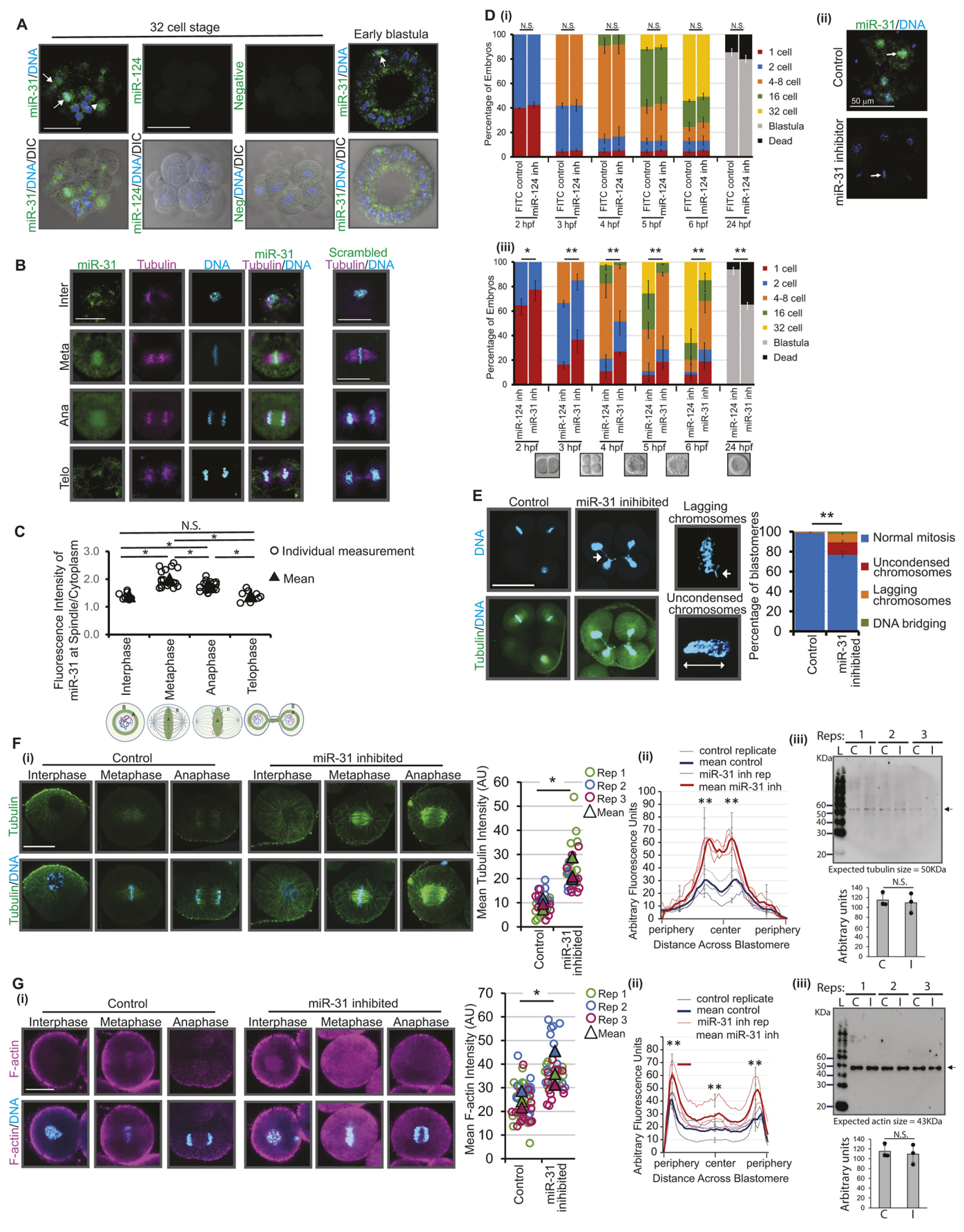


Fig. 1. See next page for legend.

Fig. 1. miR-31 localizes to the mitotic spindles in a cell-cycle dependent manner and is required for embryonic development. (A) miR-31 is located in at the mitotic spindle in dividing cells (white arrows) and perinuclearly in cells in interphase (arrowhead). Embryos (16- to 32-cell stage) were subjected to miR-31 or miR-124 FISH (green), and counterstained with Hoechst dye to detect DNA (blue). Scale bars: 50 µm. miR-124 is used as a negative control. Early blastula has miR-31 enriched in the spindle midzone (arrow). (B) Single slices of a confocal z-stack of 16- to 32-cell stage blastomeres are depicted. Embryos were hybridized with either DIG-labeled miR-31 or scrambled LNA probes (green) followed by immunolabeling with β-tubulin antibody (magenta) and counterstaining with DAPI to detect DNA (cyan). The metaphase, anaphase and telophase embryos were also hybridized with DNP-labeled β-actin probe (Meta) or Fascin probe (Ana and Telo) (not shown). Inter, interphase; Meta, metaphase; Ana, anaphase; Telo, telophase. Scale bar: 20 μm. (C) Z-stack confocal images were collected at 0.4 μm per slice for quantification. Schematic of blastomeres in various phases are illustrated with region of interest (ROI) highlighted in dark green. miR-31 is quantified using ImageJ. The ratio of miR-31 at the spindle and in the cytoplasm is measured and plotted. n=8 interphase blastomeres, 20 metaphase blastomeres, 23 anaphase blastomeres and 8 telophase blastomeres. *P≤0.05 using an ANOVA with a Tukey-Kramer post-hoc test. (D) Zygotes were injected with miR-31 inhibitor or control miR-124 inhibitor. The number of embryos in each developmental stage was recorded every 1 h for 6 h post-fertilization (hpf), then again at 24 hpf. Created with BioRender.com. (Di) miR-124 inhibitor-injected (miR-124 inh) embryos developed similarly as the FITC control-injected (FITC control) embryos. n=310 for FITC control-injected embryos and n=317 for miR-124 inhibitor-injected embryos. N.S., not significant. (Dii) Texas Red dextran or miR-31 inhibitor was injected into zygotes. 16- to 32-cell stage embryos were subjected to miR-31 FISH (green) and counterstained with DAPI for DNA (blue). White arrows indicate a dividing blastomere in metaphase. (Diii) As no apparent toxicity is observed with miR-124 inhibitor, it is used as a control for LNA toxicity. n=212 for the miR-31 inhibitor (miR-31 inh) and miR-124 LNA inhibitor control-injected (miR-124 inh) embryos; n=128 for control miR-124 inhibitor-injected embryos. *P<0.05, **P<0.01 using Cochran-Mantel-Haenszel test. Images of representative two-cell stage embryo (2 hpf), four- to eight-cell stage (4 hpf), 16-cell stage (5 hpf), 32-cell stage (6 hpf) and blastula are shown. (E) miR-31-inhibited embryos exhibit chromosomal bridging, lagging chromosomes (arrows) and uncondensed chromosomes that may result in aneuploidy. Embryos were injected with miR-31 LNA inhibitor or control miR-124 LNA inhibitor, and immunolabeled for tubulin in green and counterstained DNA with DAPI in blue. Scale bar: 50 µm. Blastomeres undergoing mitosis were scored for chromosomal abnormalities as indicated. **P<0.01 using Cochran-Mantel-Haenszel test n=138 for control miR-124 inhibitor-injected blastomeres; n=139 miR-31 inhibitor-injected embryos. Three biological replicates. (Fi) Embryos were injected with miR-31 LNA inhibitor or control miR-124 LNA inhibitor and immunolabeled for tubulin in green and counterstained DNA with DAPI (blue). The tubulin level of entire anaphase blastomere is the region of interest, where the mean fluorescence intensity (mean gray value) was determined with ImageJ. n=37 control blastomeres; n=30 miR-31-inhibited blastomeres in at least three replicates. *P<0.05 using a two-tailed Student's t-test. Scale bar: 10 µm (Fii) We also used line scans for quantification across the blastomeres in anaphase for quantification. n=29 control and n=21 miR-31inhibited blastomeres. **P≤0.05, two-tailed Student's t-test. (Fiii) Three replicates of 150 cleavage stage embryos injected with control miR-124 or miR-31 inhibitor were collected for immunoblotting, using a tubulin antibody (arrow). L, ladder; C, control; I, miR-31 inhibitor. N.S., not significant, two-tailed Student's t-test. (Gi) Control embryos exhibit enriched filamentous actin (F-actin) at the cell cortex and surrounding the chromosomes. miR-31-inhibited embryos exhibit an increase in F-actin, particularly surrounding the chromosomes. Zygotes were injected with miR-31 LNA inhibitor and labeled with Alexa647-phalloidin (magenta) and counterstained with DAPI (blue). The F-actin level of entire anaphase blastomere is the region of interest, where the mean fluorescence intensity was determined with ImageJ. n=49 controls; n=40 miR-31-inhibited blastomeres in at least three replicates. *P<0.05 using a twotailed Student's t-test. Scale bar: 10 µm (Gii) Line scans are used for quantification across the blastomeres in anaphase for quantification. n=34 for control and n=37 for miR-31-inhibited in at least three replicates. **P<0.05, twotailed Student's t-test. (Giii) Three replicates of 150 cleavage stage embryos injected with control miR-124 or miR-31 inhibitor were collected for immunoblot. The membrane used for tubulin immunoblot in Fiii was stripped and reprobed with a pan-actin antibody JLA20 (arrow). L, ladder; C, control; I, miR-31 inhibitor. N.S., not significant, two-tailed Student's t-test.

suppresses luciferase reporters containing the 3'UTRs of *Gelsolin* and *Fascin*, and the CDS and 3'UTRs of β -actin and Rab35 (Fig. 2A).

To examine whether the increase in cytoskeletal proteins induced by miR-31 inhibition may be a result of its suppression of Fascin and/or Rab35 mRNA, we injected Fascin and Rab35 target protectors (TPs) into zygotes (Staton and Giraldez, 2011; Remsburg et al., 2019). TPs are morpholino antisense oligonucleotides (MASOs) designed to block the binding of miR-31 to the 3'UTR of Fascin and Rab35 (Fig. 2B,E). By including nucleotides flanking the validated miR-31 binding site, TPs bind specifically to the Fascin and Rab353' UTR. Both Fascin and Rab35 TP-injected cleavage stage embryos (16-32 cells) exhibit more chromosomal defects compared with controls (Fig. 2B,E), similar to what we observe in miR-31-inhibited embryos (Fig. 1E). Additionally, Fascin TP-injected cleavage stage embryos (16-32 cells) exhibit a significant increase in both tubulin and F-actin compared with controls (Fig. 2C,D), similar to miR-31inhibited embryos (Fig. 1F,G). However, Rab35 TP-injected cleavage stage embryos exhibit no change in tubulin or F-actin levels compared with controls (Fig. 2F,G).

Spatial distribution of miR-31 and its targets on the mitotic spindle is evolutionarily conserved between sea urchin embryos and mammalian cells

As miRNAs must bind to their target RNAs to mediate post-transcriptional regulation (Bartel, 2018), we examined where and when miR-31 interacts with its targets in the sea urchin embryo. We observed that β -actin, Gelsolin, Rab35 and Fascin mRNAs co-localize with miR-31 on the mitotic spindle during mitosis (Fig. 3A). During interphase and prophase, miR-31 and its targets localize to the perinuclear region (Figs 3A and 1C). During metaphase and anaphase, miR-31 and its targets localize to the midzone of the mitotic spindle (Figs 3A and 1A,C). Interestingly, miR-31 target transcripts Fascin, Rab35 and Gelsolin appear to be at the presumptive midbody (Fig. 3A).

To determine whether this localization is evolutionarily conserved, we examined the spatial localization of miR-31 and its target mRNAs Fascin and Rab35 in HCT116 (human colon cancer cells), which is known to have upregulated miR-31 (Cekaite et al., 2012) and LLC-PK (pig kidney) cells, as these have previously been used to observe RNA localization during mitosis (Remsburg et al., 2023; Hull et al., 1976). We observed miR-31 and its target mRNAs localize to the spindle midzone in anaphase of these cells (Fig. 3B,C). Interestingly, these RNAs do not localize to the metaphase plate in HCT116 cells. However, in anaphase and telophase, these transcripts localize to the spindle midzone in HCT116 and LLC-PK cells, similar to the sea urchin embryos. This result indicates that there may be a temporal difference in the subcellular transport of these RNAs to the spindle midzone, but the co-localization of miR-31, Fascin and Rab35 mRNA is evolutionarily conserved between the sea urchin embryo and mammalian cells.

De novo translation occurs at the mitotic spindle during mitosis

Co-localization of miR-31 and its target RNAs lead to our hypothesis that miR-31 post-transcriptionally regulates its targets at the mitotic spindle. To test this hypothesis, we identified EEF1A1, a translation elongation protein, at the mitotic spindle (Fig. 4A) (Chassé et al., 2019). As we observe translational machinery and *Fascin* mRNA at the mitotic spindle, we hypothesize that *Fascin* is translated at the mitotic spindle. We used the puromycin proximity ligation assay (PuroPLA) assay, which allows us to observe newly translated Fascin (Chin and Lécuyer, 2021). We

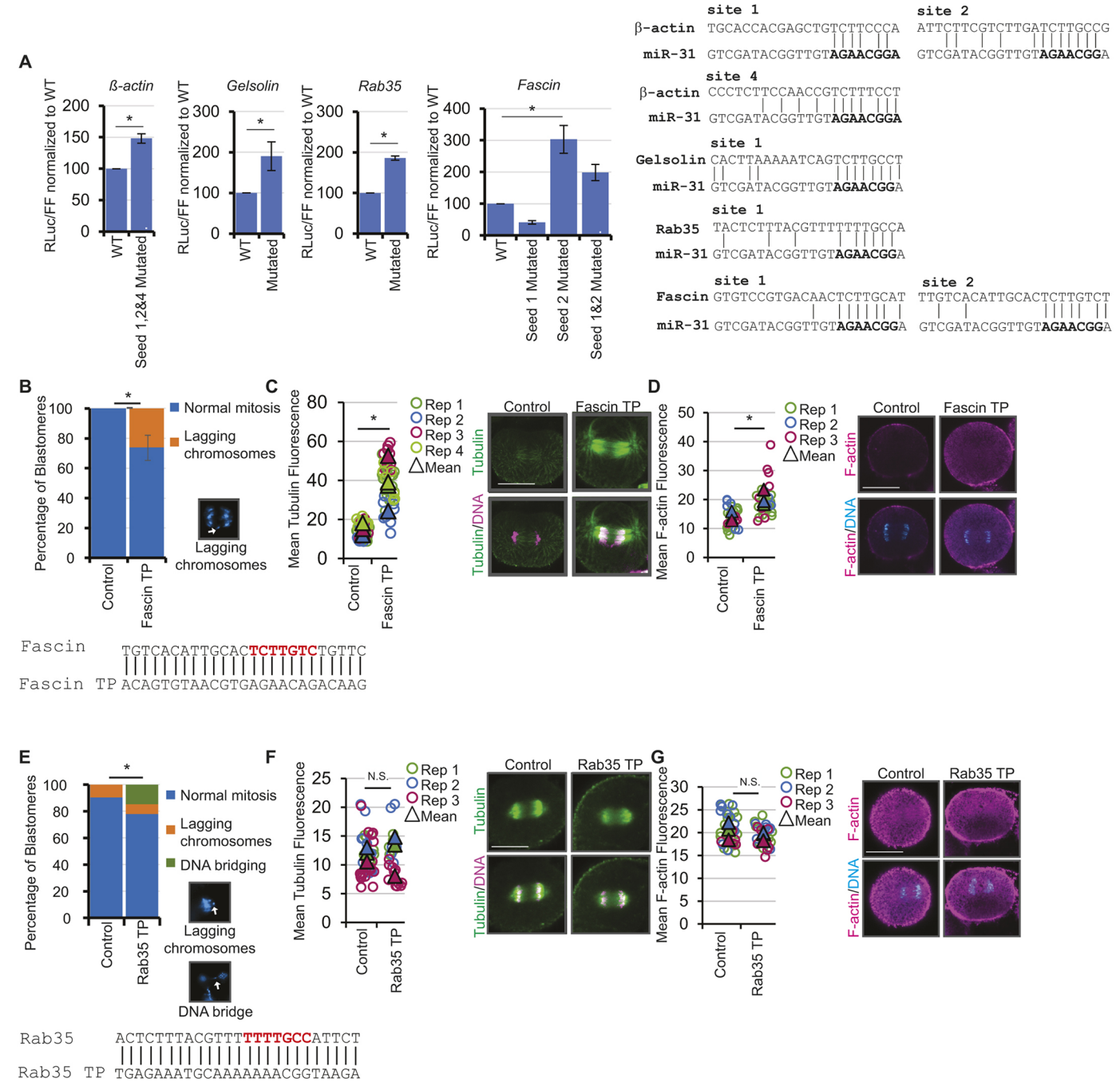


Fig. 2. Identification and validation of miR-31 targets. (A) Potential targets were cloned downstream of Renilla luciferase (RLuc). Mutagenesis was performed on the predicted miR-31 seed sequences. After the constructs were in vitro transcribed and microinjected into zygotes, along with firefly luciferase (FF) as a normalization control, the embryos were collected and lysed 24 hpf and assayed. *P≤0.05 using a two-tailed Student's t-test for β-actin, Rab35 and Fascin, and a one-tailed Student's t-test for Gelsolin. Data are mean±s.e.m. Alignments of transcript 3'UTRs and the miR-31 sequence are depicted, with miR-31 seed sequence in bold. (B) Blastomeres from 16- to 32-cell stage embryos undergoing mitosis were scored for chromosomal abnormalities, as indicated. Fascin TP-injected embryos exhibit lagging chromosomes. *P≤0.05 using CMH. Fascin TP is designed to block miR-31 seed sequence (red), as determined by site-directed mutagenesis and luciferase assays. BLASTN determined Fascin TP to only have homology to the Fascin transcript. (C) Cleavage stage embryos were immunolabeled for tubulin (green) and counterstained with DAPI for DNA (magenta). ImageJ was used to measure the fluorescence intensity of individual blastomeres during anaphase. *P≤0.05 using a two-tailed Student's t-test. Scale bar: 10 µm. (D) Cleavage stage embryos were labeled with Alexa647-phalloidin for actin (magenta) and counterstained with DAPI (cyan). *P≤0.05 using a two-tailed Student's t-test. (E) Cleavagestage blastomeres undergoing mitosis were scored for chromosomal abnormalities as indicated. Rab35 TP-injected embryos exhibit DNA bridges and lagging chromosomes that may result in aneuploidy. *P<0.05 using a two-tailed Student's t-test. Rab35 TP is designed to block miR-31 seed sequence (red), as determined by site-directed mutagenesis and luciferase assays. BLASTN determined Rab35 TP to have homology to only the Rab35 transcript. (F) Cleavage-stage embryos were injected with control or Rab35 TP, immunolabeled for tubulin (green) and counterstained with DAPI for DNA (magenta). Rab35 TP-injected embryos exhibit no change in tubulin. ImageJ was used to measure the fluorescence intensity of individual blastomeres during anaphase. N.S., not significant (P>0.05 using a two-tailed Student's t-test). Scale bar: 10 µm (G) Zygotes were injected with control or Rab35 TP, labeled with Alexa647-phalloidin and counterstained with DAPI for DNA. Rab35 TP-injected cleavage stage embryos exhibit no change in F-actin. ImageJ was used to measure the fluorescence intensity of single blastomeres in anaphase. N.S., not significant (P>0.05 using a two-tailed Student's t-test). Scale bar: 10 µm.

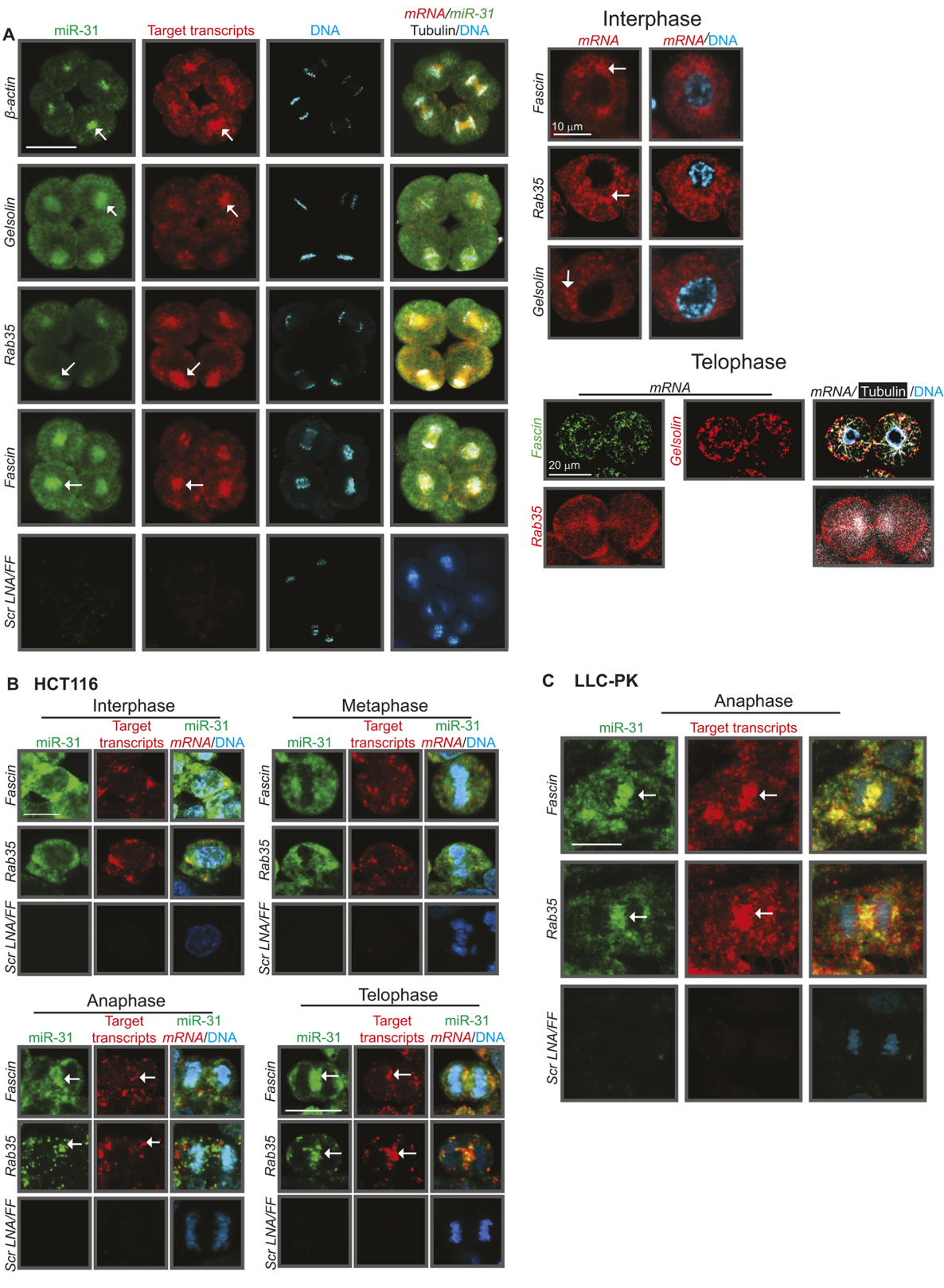


Fig. 3. miR-31 and its target transcripts co-localize to the mitotic spindles. (A) Eight- to 16-cell stage embryos were subjected to double FISH (green for miR-31 and red for target transcript) followed by immunolabeling with β-tubulin antibody (white) and counterstained DNA with DAPI (blue). Negative controls are a scrambled LNA and a DNP-labeled Firefly (FF) RNA probe. Scale bars: 50 μm, unless otherwise stated. For interphase blastomeres, embryos were subjected to FISH (red for target transcript) and counterstained with DAPI (blue). For telophase blastomeres, embryos were subjected either to double FISH with *Fascin* in green and *gelsolin* in red, or to a single FISH with *Rab35* in red, followed by immunolabeling with β-tubulin antibody (white) and counterstaining of DNA with DAPI (blue). (B) miR-31 and *Fascin* RNA localize between dividing human colon cancer cells (HCT116) (arrow). A scrambled miR LNA probe (scr LNA) and Firefly probe (FF) are used as negative controls. Scale bars: 10 μm. (C) miR-31 and *Fascin* RNA localize between dividing pig kidney epithelial cells (LLC-PK) (arrows). A scrambled miR LNA probe and Firefly probe are used as a negative control. Scale bar: 10 μm.

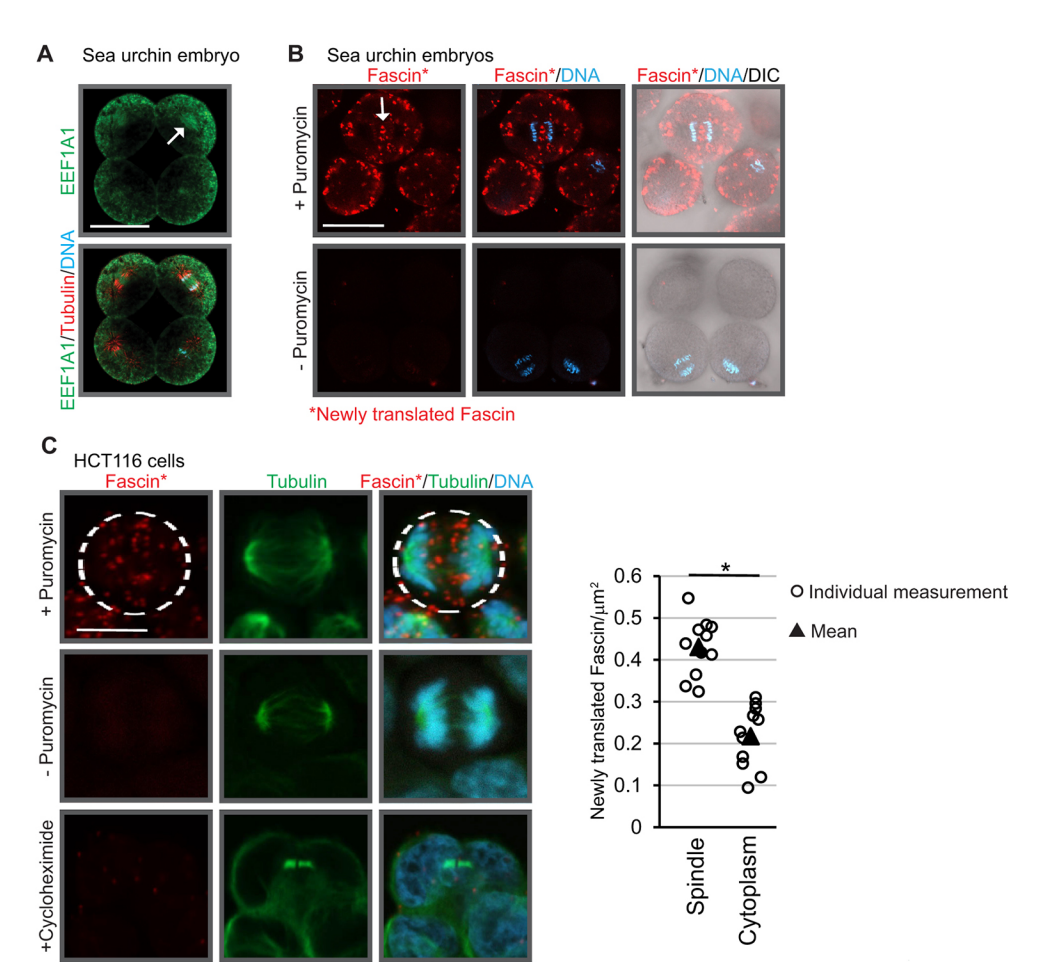


Fig. 4. Translational components and newly translated proteins are localized to the mitotic spindle. (A) EEF1A1, a peptide elongating factor, is observed at the mitotic spindle. Embryos were immunolabeled with an FF1A1 (green) and a tubulin antibody (red), then DNA was counterstained with DAPI (blue). Scale bar: 50 µm. (B) 16- to 32-cell stage embryos were treated with the DuoLink PuroPLA assav with newly translated Fascin in red, then counterstained with DAPI (DNA in blue). Newly translated Fascin (red) is observed at the cell cortex and mitotic spindle in early cleavage stage blastomeres. Scale bar: 50 µm. (C) HCT116 cells were treated with the DuoLink PuroPLA assay with newly translated Fascin in red, then immunolabeled with an Alexa-488conjugated tubulin antibody in green and counterstained with DAPI (DNA in blue). The measured spindle region of interest is indicated by the white dotted line, where the mean fluorescence intensity was determined. The cytoplasmic region is outside the dotted area within the cell. *n*=11 anaphase cells in at least three replicates. *P<0.05 using a two-tailed Student's t-test. Scale bar: 5 µm.

observed *de novo* translation of Fascin at the cell periphery and mitotic spindle of dividing sea urchin blastomeres (Fig. 4B). In HCT116 cells, we observed significantly more newly translated Fascin at the anaphase mitotic spindle compared with the cytoplasm. This result suggests that active translation of Fascin at the mitotic spindle is evolutionarily conserved.

*Newly translated Fascin

$\operatorname{miR-31}$ inhibition results in more Rab35 and Fascin protein at the mitotic spindle

As miRNAs are post-transcriptional regulators that generally negatively mediate gene expression of their target transcripts (Bartel, 2018), we used PuroPLA to test whether inhibiting miR-31 in the embryo would affect the level of newly translated protein made from miR-31 target transcripts. We observe an increased trend of more newly translated Fascin protein in the cytoplasm of miR-31-inhibited embryos compared with the control embryos (Fig. 5A). Importantly, the newly translated Fascin is significantly increased at the mitotic spindle in miR-31-inhibited embryos compared with the control embryos, highlighting that miR-31 regulates local translation of *Fascin* (Fig. 5A).

Using conventional immunolabeling in fixed embryos, we also observe a significant increase of Fascin and Rab35 protein at the mitotic spindle in miR-31-inhibited embryos compared with control embryos (Fig. 5B,D, Fig. S2). Furthermore, specifically inhibiting the binding of miR-31 to *Fascin* mRNA (with Fascin TP) or *Rab35* mRNA (with Rab35 TP) also resulted in a significant increase of their protein levels at the mitotic spindle (Fig. 5C,E). Importantly, this localization of increased Fascin and Rab35 proteins at the

mitotic spindle corresponds to the localization of miR-31, *Fascin* and *Rab35* mRNA transcripts (Figs 1 and 3). These data suggest that miR-31 post-transcriptionally regulates *Fascin* and *Rab35* mRNA at the mitotic spindle.

Local translation of Fascin is important for embryonic development

As our data indicate that miR-31 along with its target transcripts and proteins have a subcellular localization on the mitotic spindle and that inhibiting miR-31 leads to increased Fascin and Rab35 protein levels (Figs 3 and 5), we tested the importance of local translation of Fascin during early development (Fig. 6A). We tested this by forcing Fascin translation to occur at the cell membrane, in the background of depleted Fascin protein. In this set of experiments, four conditions were tested. In all conditions, the zygotes were injected with prenylated mCherry-PP7 coat protein which localizes to the cell membrane. For the negative control, we co-injected zygotes with control MASO and mRNA consisting of a plasmid sequence fused with PP7 stem loop structure (referred to as Neg-PP7 mRNA) that binds to mCherry-PP7 coat protein at the cell membrane (Fig. 6Ai). These control embryos are able to make Fascin protein from endogenous Fascin mRNA enriched at the spindle (Fig. 6Ai,B.C). To deplete Fascin protein, we injected zygotes with Fascin MASO (Fig. 6Aii). In these embryos, the endogenous Fascin mRNA is not translated into Fascin proteins due to MASO binding (Fig. 6Aii,B,C), resulting in a significant depletion of Fascin protein. To test the specificity of the Fascin MASO, we co-injected zygotes with Fascin MASO and Fascin coding sequence (CDS) mRNA

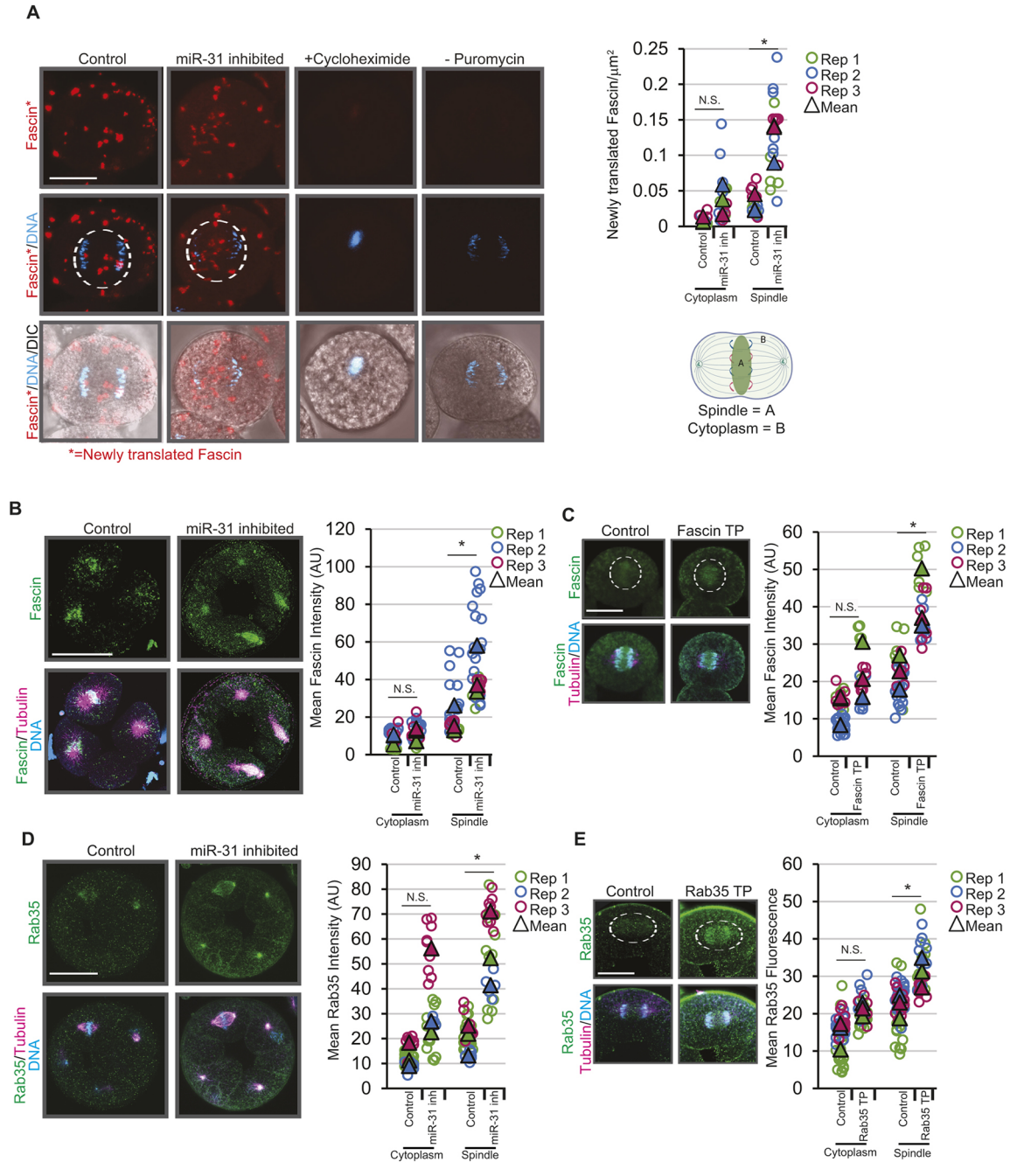
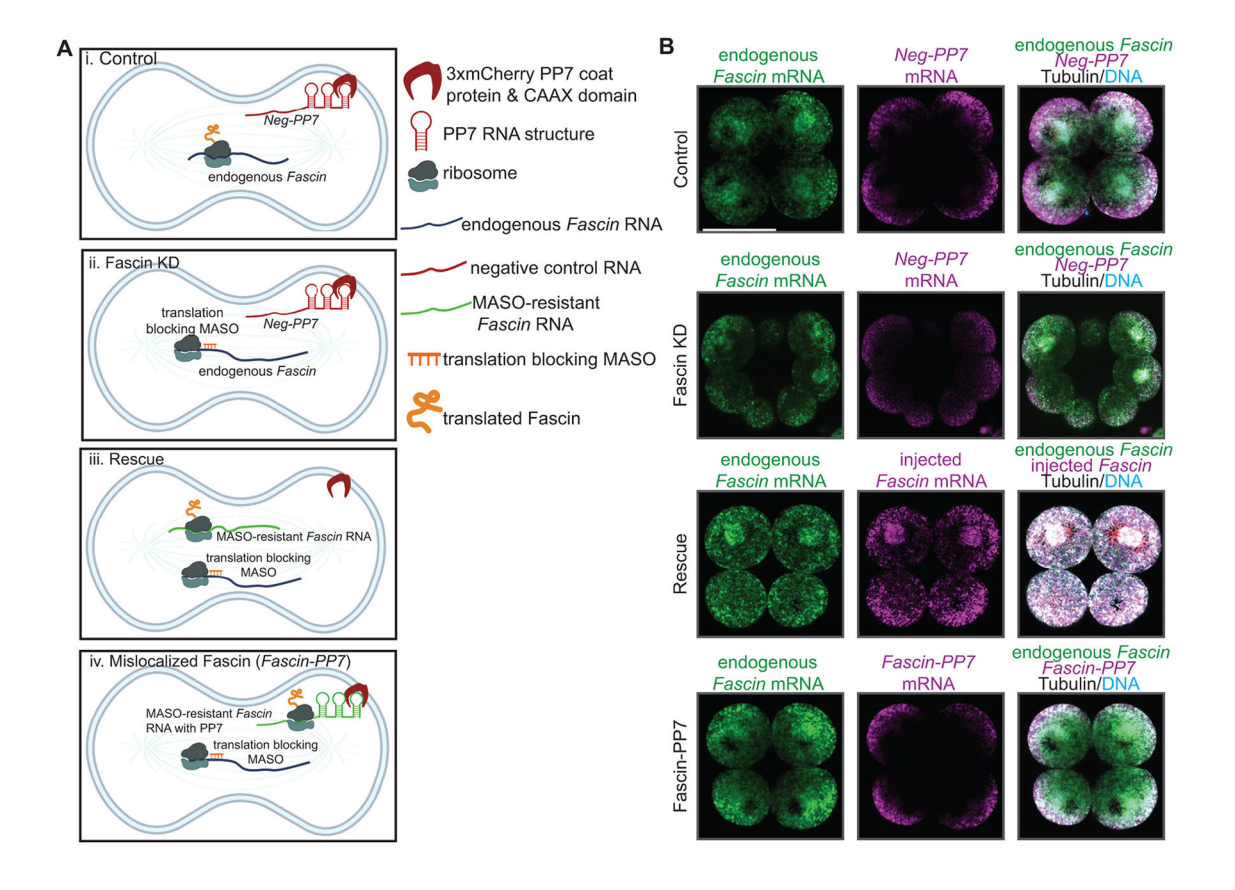


Fig. 5. miR-31 inhibition results in increased Fascin and Rab35 protein. (A) Control or miR-31-inhibited 16- to 32-cell stage embryos were treated with the DuoLink PuroPLA assay with newly translated Fascin in red, and DNA was counterstained with DAPI (in blue). The density of newly translated Fascin molecules is significantly higher at the spindle (indicated by the white dotted lines) in miR-31-inhibited embryos compared with control embryos. A maximum intensity projection of five z-slices taken at 1 µm intervals that surrounds and includes the chromosomes was created for each image. Individual red dots observed in the spindle region and in the cytoplasmic region were counted. The number of dots were divided by the area. n=16 control blastomeres; n=18 miR-31-inhibited blastomeres in three replicates. *P≤0.05 using a two-tailed Student's t-test. Scale bar: 10 μm. Created with BioRender.com. (B) Embryos were injected with a control miR-124 LNA inhibitor or a miR-31 LNA inhibitor and immunolabeled with Fascin antibody (green) and tubulin antibody (magenta) followed by DAPI counterstaining of DNA (blue). Image J was used to measure the mean fluorescence at the spindle (region A in the schematic depicted in A) and in the cytoplasm (region B in the schematic) of anaphase blastomeres. AU, arbitrary units. n=29 control blastomeres, n=32 miR-31inhibited blastomeres. *P<0.05 using a two-tailed Student's t-test. Scale bar: 50 µm. (C) Embryos were injected with Fascin TP to remove the suppression of Fascin by miR-31. Fascin TP-injected embryos were immunolabeled with Fascin antibody. ImageJ was used to measure the fluorescence intensity of individual blastomeres during anaphase as described in the schematic in A. n=34 control blastomeres; n=23 Fascin TP blastomeres. *P<0.05 using a twotailed Student's t-test. Scale bar: 10 µm. White dotted lines indicate the spindle midzone. (D) Embryos were injected with control miR-124 LNA inhibitor or miR-31 LNA inhibitor, and immunolabeled with Rab35 antibody (green) and tubulin antibody (magenta), followed by DAPI counterstaining for DNA (blue). n=39 control blastomeres; n=27 miR-31-inhibited blastomeres. *P≤0.05 using a two-tailed Student's t-test. Scale bar: 50 μm (E) Embryos were injected with Rab35 TP to remove the suppression of Rab35 by miR-31. Rab35 TP-injected embryos were immunolabeled with Rab35 antibody. ImageJ was used to measure the fluorescence intensity of individual blastomeres during anaphase. n=50 control blastomeres; n=31 Rab35 TP blastomeres. * $P \le 0.05$ using a two-tailed Student's t-test. Scale bar: 10 µm. White dotted lines indicate the spindle midzone.



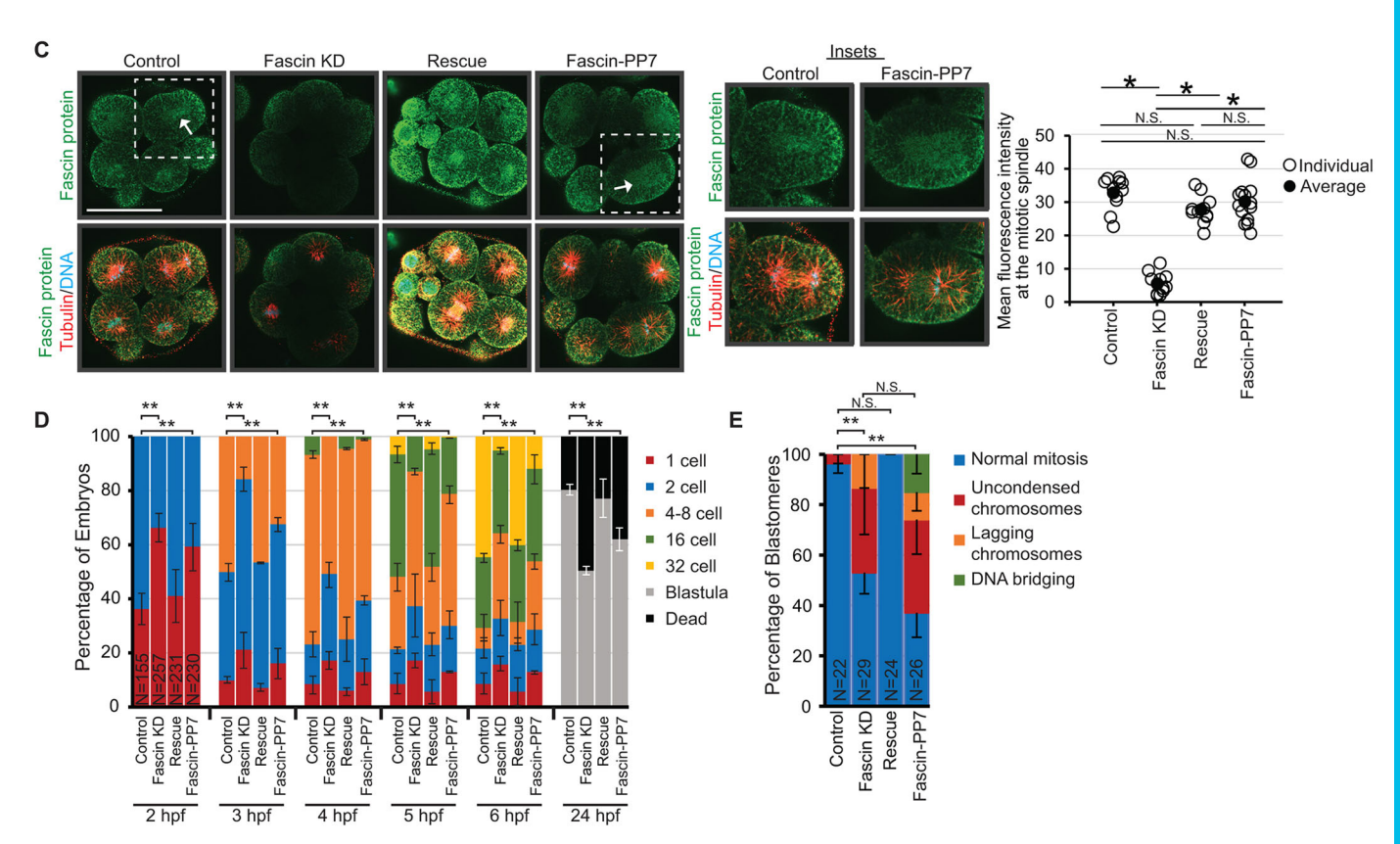


Fig. 6. See next page for legend.

Fig. 6. Local translation of Fascin at the mitotic spindle is important for proper cell division. (A) Schematic of components injected for testing the importance of local translation of Fascin at the mitotic spindle. All zygotes were injected with the prenylated mCherry PP7 coat protein. (i) Control embryos were also injected with control MASO and a negative control RNA fused to PP7 repeats (Neg-PP7). Endogenous Fascin mRNA is localized at the spindle and can be translated normally. (ii) Fascin KD embryos were injected with Fascin MASO and Neg-PP7. Endogenous Fascin transcript is localized at the spindle but cannot be translated due to Fascin MASO binding and inhibiting its translation. (iii) Rescue embryos were injected with Fascin MASO and Fascin MASO-resistant Fascin CDS+3'UTR. The endogenous Fascin localizes to the spindle, but cannot be translated due to Fascin MASO binding; however, the exogenous Fascin CDS+3'UTR localizes to the spindle and can be translated. (iv) Fascin-PP7 embryos were injected with Fascin MASO and Fascin MASO-resistant Fascin CDS RNA fused to PP7 repeats. Endogenous Fascin localizes to the spindle but cannot be translated due to the Fascin MASO, but exogenous Fascin localizes to the cell membrane due to the PP7 repeats, forcing translation of Fascin to occur at the cell membrane. Created with BioRender.com. (B) Embryos were injected as described in A and fixed. Fascin transcripts (green) and exogenously injected transcripts, either Neg-PP7 or Fascin-PP7 (magenta), were detected in these embryos. Embryos were also immunolabeled using tubulin antibody (white). DNA (blue) is counterstained with DAPI. Scale bar: 50 µm. (C) Zygotes were injected as described in A. 16- to 32-cell cleavage-stage embryos were immunolabeled for Fascin protein (green) and tubulin (red), and counterstained with DAPI for DNA (blue). The white arrows indicate Fascin protein enrichment. The areas outlined on the left are shown on the right depicting Fascin in individual blastomeres. Fascin protein levels at the mitotic spindle in control, Fascin KD, rescue and Fascin-PP7 are quantified in anaphase blastomeres, with the region of interest around the spindle area. n=11 for control, Fascin KD and rescue; n=14 for Fascin-PP7. *P≤0.05 using a two-tailed Student's t-test. Three biological replicates. Scale bar: 50 μm. (D) Zygotes were injected with components as depicted in A. The number of embryos at each stage was recorded every 1 h for 6 hpf, then again at 24 hpf. No significant difference was observed between the control and rescue groups at all time points. **P<0.01 using a Cochran-Mantel-Haenszel test. (E) Zygotes were injected as described in A. Blastomeres undergoing mitosis were scored for

lacking Fascin MASO-binding sequence (Fig. 6Aiii). As expected, the endogenous and exogenous *Fascin* mRNAs are both localized to the spindles (Fig. 6Aiii,B).

chromosomal abnormalities. **P<0.01 using Cochran-Mantel-Haenszel

conducted in three biological replicates.

statistical test was used; N.S., not significant (P>0.05). All experiments were

In these Fascin knockdown (KD) embryos, the injected MASOresistant Fascin mRNA is translated to protein at the spindle (Fig. 6B,C). These results indicate that Fascin MASO is specifically blocking Fascin translation, as we are able to restore Fascin protein expression with the exogenous Fascin mRNA, resulting in a similar level of Fascin protein in control and the rescued embryos (Fig. 6C). To test the importance of local translation of Fascin, we co-injected Fascin MASO with Fascin CDS mRNA recalcitrant to Fascin MASO binding fused to PP7 (Fig. 6Aiv). In these embryos, the Fascin mRNA containing the PP7 will bind to mCherry-PP7 coat protein at the cell membrane; these we refer to as Fascin-PP7 embryos (Fig. 6Aiv). In these Fascin-PP7 embryos, the majority of the endogenous Fascin mRNA at the spindle fails to be translated due to Fascin MASO, and the source of Fascin protein in the embryo comes from the exogenously injected Fascin mRNA sequestered at the cell membrane (Fig. 6B). In Fascin-PP7 embryos, we observe that Fascin mRNA is enriched at the spindle with a more diffuse localization, containing both endogenous and injected Fascin mRNA (Fig. 6B). Interestingly, in these Fascin-PP7 embryos, Fascin protein is localized at the cell membrane, with a wider distribution around the mitotic spindle (astral microtubules and midzone) instead of being enriched at the

spindle midzone (Fig. 6C). This indicates that the localization of Fascin protein depends on the subcellular localization of its transcripts.

To test the importance of local translation of Fascin in early development, we followed embryos injected with these four treatments through early development where we tabulated the percentage of embryos at a particular stage for 24 h (Fig. 6D). Consistent with our previous study (Testa et al., 2023), we observed that Fascin MASO-injected embryos have a significant delay in development as early as 2 hpf, where 60% of control embryos reach the two-cell stage, but only 34% of Fascin KD embryos have undergone the first division (Fig. 6D). This developmental defect persists to 24 hpf. When endogenous Fascin translation is blocked with a MASO, but exogenous MASO-resistant Fascin mRNA is supplemented (Fig. 6D), the developmental defect in Fascin KD embryos is rescued. However, intriguingly, Fascin-PP7 embryos experience a significant delay in development, as early as 2 hpf, when only 40% of Fascin-PP7 embryos have divided into two cells. Importantly, this developmental difference persists to the blastula stage (Fig. 6D). Additionally, we observe significantly more chromosomal defects in Fascin KD and Fascin-PP7 embryos compared with control and Fascin rescue embryos (Fig. 6E). Overall, results support the idea that the localized translation of Fascin is important for cell division during early embryonic development.

DISCUSSION

The early cleavage stage of development is a crucial time point that requires exquisite protein regulation, as the embryo undergoes rapid rounds of cell division where precise regulation of the mitotic proteome is required for proper chromosomal segregation (Siefert et al., 2015; Orth et al., 2012). We have identified miR-31, an evolutionarily conserved miRNA present in all metazoans, as playing an important role in regulating the early cleavage stage sea urchin embryos. miR-31, along with four of its validated targets, β -actin, Gelsolin, Rab35 and Fascin mRNAs, have an evolutionarily conserved localization to the mitotic spindle in the sea urchin embryo and mammalian cells (Figs 1 and 3), suggesting that the regulatory paradigm of miR-31 at the mitotic spindle may be conserved.

The function of miR-31 has been examined in myogenesis, bone homeostasis and skeletogenesis, and in the context of cancer (Su et al., 2020; Stepicheva and Song, 2015; Crist et al., 2012; Cekaite et al., 2012; Lv et al., 2017; Mizoguchi et al., 2013; Ge et al., 2017; Tian et al., 2017; Zheng et al., 2021). In the sea urchin embryo, miR-31 regulates components of the skeletogenic GRN and its inhibition leads to skeletal defects in the gastrula (Stepicheva and Song, 2015; Sampilo et al., 2021). Thus far, miR-31 has not been examined in the context of mitosis or early dividing embryos. Our results indicate that miR-31 perturbation in the sea urchin embryo results in significant developmental delay, in lethality with chromosomal defects (DNA bridging and lagging chromosomes) and in increased cytoskeleton polymerization (Fig. 1D-G).

We observed increased polymerized tubulin levels using immunofluorescence but no change in monomeric tubulin levels using western immunoblot in miR-31-inhibited embryos compared with the control (Fig. 1Fi,ii,iii). Given the same amount of tubulin subunits *in vitro*, polymerized tubulin appears brighter than unpolymerized tubulin, owing to coalesced fluorophores (Colin et al., 2018). Therefore, the total level of tubulin may not have altered, but miR-31 inhibition promotes the polymerization of tubulin via an unknown mechanism.

Chromosomal defects observed in miR-31 inhibitor-injected embryos may be in part due to increased tubulin polymerization, as tubulin dynamics must be carefully regulated to ensure faithful chromosome segregation during mitosis (Lin et al., 2020). These chromosomal defects can lead to aneuploidy and cell cycle arrest (Santaguida and Amon, 2015). In turn, cell cycle arrest could result in the developmental arrest, delay and death that we observe in miR-31-inhibited embryos (Fig. 1D).

miR-31 inhibition also leads to increased F-actin (Fig. 1G). We found miR-31 directly suppresses β -actin (Fig. 2A). For cytoskeletal actin, we observed that filamentous actin, detected with phalloidin staining, is significantly increased; however, no change is observed in monomeric actin levels using western immunoblot in miR-31inhibited embryos compared with the control (Fig. 1Gi,ii,iii), suggesting that miR-31 inhibition promotes formation of filamentous actin. Actin can be polymerized either spontaneously or mediated by Arp2/3 or Formin family members (Pollard, 2016). The increase in F-actin in miR-31-inhibited embryos may also be an indirect effect, as miR-31 directly suppresses other transcripts encoding proteins that modulate cytoskeletal dynamics, such as Fascin, Rab35 or Gelsolin (Fig. 2A), which in turn may promote formation of F-actin in the embryo. In support of this idea, removal of the direct suppression by miR-31 of Fascin results in significant increase of F-actin (Fig. 2D). As actin plays several other roles during mitosis, increased actin from miR-31 perturbation may negatively impact mitosis. For example, actin polymerization provides forces that separate the newly duplicated centrosomes to opposite sides of the nucleus, immediately before nuclear envelope breakdown (Cao et al., 2010). Actin also facilitates initial chromosome congression, by forming a shell with Myosin II around the nucleus that contracts immediately after nuclear envelope breakdown to reduce the chromosomal volume and facilitate access the kinetochores for spindle microtubules (Booth et al., 2019). Actin also interacts with microtubules at the cell cortex to mediate spindle orientation (Yu et al., 2019) as well as cytokinesis (Addi et al., 2018). Additionally, perturbation of actin dynamics results in shorter spindles and prolonged mitosis (Kita et al., 2019). Thus, correct actin dynamics are important for mitosis. In addition, the increase in F-actin we observe in miR-31-inhibited embryos may disrupt various aspects of mitosis (Fig. 1Gi,ii) and potentially contribute to miR-31 inhibitorinduced developmental defects.

Other direct targets of miR-31 that regulate cytoskeletal dynamics include Gelsolin, Rab35 and Fascin mRNAs (Fig. 2A). Gelsolin severs and caps actin filaments (Feldt et al., 2019). Although many studies have examined the function of Gelsolin in the context of cancer, inflammation and amyloidosis (Hsieh and Wang, 2022; Feldt et al., 2019), its function during mitosis remains elusive. Rab35 encodes a GTPase that is involved in endosomal protein trafficking and regulation of actin dynamics (Chesneau et al., 2012; Remsburg et al., 2021). Besides its function in the formation of the cytokinetic furrow (Klinkert et al., 2016; Remsburg et al., 2021; Chesneau et al., 2012), The role of Rab35 during mitosis is limited. We found that removing the direct suppression of Rab35 by miR-31 using Rab35 TP results in increased Rab35 protein and chromosomal defects (Figs 2E and 5E); however, Rab35 TP results in no change in microtubules or F-actin levels compared with the controls (Fig. 2F,G). Thus, the direct suppression by miR-31 of Rab35 impacts chromosome segregation independently of cytoskeletal changes. Rab35 has been shown to mediate endocytosis of excess plasma membrane in cell shape changes (Jewett et al., 2017) and cytokinesis (Chesneau et al., 2012). We hypothesize that increased levels of Rab35 protein in Rab35 TP-injected embryos may result in

precocious cytokinesis that can lead to unresolved DNA bridges, resulting in DNA damage and embryonic lethality (Petsalaki and Zachos, 2021). However, the exact mechanism of how increased Rab35 results in chromosomal segregation defects is unclear.

Fascin is an actin bundling protein that also interacts with and directs polymerization of microtubules (Villari et al., 2015; Zanet et al., 2012; Otto et al., 1980). We observed that miR-31 inhibition and removal of the direct suppression of Fascin by miR-31 resulted in significant increases in Fascin protein, tubulin and F-actin (Figs 5B,C and 2C,D). Although Fascin protein is abundant in newly fertilized zygotes, it is significantly decreased at the two-cell stage (Testa et al., 2023), which is consistent with our findings that blocking Fascin translation immediately after fertilization does result in reduced Fascin protein, as well as developmental defects and chromosomal abnormalities by the 16- to 32-cell stage (Fig. 6C-E). Consistent with our findings, MDA-MB-231 cancer cells have Fascin overexpression that results in increased microtubule dynamics and is associated with increased metastatic potential (Heinz et al., 2017). Furthermore, Fascin KD HeLa cells have microtubules that are more stable (Villari et al., 2015). Interestingly, we observe Fascin transcript to be perinuclear in interphase sea urchin blastomeres and on mitotic spindle in dividing blastomeres and mammalian cells (Figs 3 and 6B). The level of newly translated Fascin protein at the mitotic spindle is significantly increased in miR-31-inhibited sea urchin embryos (Fig. 5A,B), which can potentially impact cell division in several ways. Nuclear Fascin has been shown to regulate intranuclear actin dynamics (Kelpsch et al., 2016; Lawson et al., 2022). Fascin also regulates cancer cell survival by binding to histone H3 to enhance chromatin compaction and recruiting the DDR factor yH2AX to damaged DNA foci to facilitate the DNA damage response (Lawson et al., 2022). We showed that perturbation of Fascin results in significant chromosomal segregation defects, and leads to developmental delay and arrest early in development (Figs 2B) and 6D,E). The ability and potential of Fascin to modulate the cytoskeleton in the local environment of the mitotic spindle, to regulate intranuclear actin dynamics and to mediate DNA damage repair make it an important protein during mitosis.

Earlier literature has shown that Rab35 functionally interacts with Fascin (Zhang et al., 2009; Remsburg et al., 2021). The overexpression of Fascin can rescue Rab35 KD phenotypes in bent bristles of fruit flies and gastrulation defects in the sea urchin embryo (Zhang et al., 2009; Remsburg et al., 2021), indicating that the functional interaction of Rab35 with Fascin is evolutionarily conserved. Interestingly, we observe that both Rab35 and Fascin co-localize to the mitotic spindle with miR-31 and are responsive to miR-31 inhibition, suggesting their potential functional interaction at the spindle. Therefore, Rab35 may regulate mitosis via its interaction with Fascin at the mitotic spindle.

Our observation that newly translated Fascin occurs in the spindle in both dividing sea urchin blastomeres and mammalian cells suggest that Fascin may perform an evolutionarily conserved and essential function during mitosis (Fig. 4). Furthermore, we demonstrate that local translation of Fascin is crucial for proper early development of the sea urchin embryo (Figs 5 and 6). In the embryonic context, when Fascin translation is forced to the cell membrane (Fascin-PP7), these embryos do not survive as well as control or Fascin-rescued embryos (Fig. 6D). As Fascin-rescued and Fascin-PP7 embryos have the same amount of exogenous *Fascin* mRNA supplied, the developmental delays observed in Fascin-PP7 embryos is not due to a relative defect or to overexpression of exogenous *Fascin* RNA (Fig. 6). Previous work has shown that the addition of the PP7 motifs to RNAs does not appear to affect

the efficacy of translation (Yan et al., 2016). Additionally, the level of Fascin protein in control versus *Fascin-PP7* transcript-injected embryos is not significantly different, suggesting that there is not a reduced amount of protein translation (Fig. 6C). We cannot rule out the possibility that sequestration of Fascin protein in the actin-rich milieu of the cell cortex is not contributing to the observed developmental delays. Interestingly, embryos with mislocalized Fascin have a higher survival rate than Fascin KD embryos. This may be due to the fact that, although Fascin translation is forced to occur at the cell membrane, some Fascin can be transported from the cell periphery to the mitotic spindle, or that Fascin KD is not complete. This is supported by our observation that, in control embryos, Fascin localizes to the spindles during mitosis; however, in Fascin-PP7 embryos, Fascin protein has a more diffuse localization at the spindle midzone, as well as at the astral microtubule (Fig. 6C).

Evidence suggesting that translation occurs on the mitotic spindle has been around for some time (reviewed by Waldron and Yajima, 2020). The first evidence indicated that actively translating ribosomes interacted with the mitotic apparatus and, later, specific mRNAs that interact with the mitotic spindle were identified (Lenk et al., 1977; Blower et al., 2007). CyclinB and Vasa mRNA have been suggested to be locally translated at the mitotic spindle (Groisman et al., 2000; Fernandez-Nicolas et al., 2022). As mitosis requires that numerous proteins function together at the correct space and time within the cell in order to faithfully segregate daughter chromosomes (Prosser and Pelletier, 2017), regulation of local translation by miR-31 at the mitotic spindle may be another mechanism through which the embryo mediates efficient protein translation to regulate spindle dynamics. A failure to control local translation of Fascin at the right time and in the right place results in severe chromosomal defects (Fig. 6). The mammalian midbody, which is assembled during mitosis, harbors translational regulators, RNA-processing proteins and mRNAs that are translated into proteins involved in cell fate, oncogenesis and pluripotency (Park et al., 2023; Skop et al., 2004; Peterman et al., 2019; Rai et al., 2021; Addi et al., 2020; Capalbo et al., 2019). We suggest that select RNAs are subcellularly transported to the spindle (Figs 1B and 3) and locally translated by metaphase (Figs 4B and 5A). Importantly, these RNAs and proteins enriched at the mitotic spindle may be incorporated into the midbody and midbody remnants that potentially play a role in cell differentiation.

Our working model is that miR-31 and its target transcripts localize to the mitotic spindle, where miR-31 dynamically regulates translation of its targets during mitosis (Fig. 7). As many transcripts that are localized to the mitotic spindle encode proteins that regulate mitosis (Blower et al., 2007; Hassine et al., 2020; Pascual et al., 2021; Remsburg et al., 2023), we propose that miR-31 regulates β actin, Gelsolin, Rab35 and Fascin to mediate actin dynamics and microtubule polymerization in order to ensure precise chromosomal segregation and a timely progression through mitosis. In postembryonic cells and cell lines, miRNAs typically inhibit translation of their targets through recruitment of deadenylases to destabilize their target transcripts (Bartel, 2018). However, in pre-blastula stage zebrafish embryos, the regulatory landscape favors translational inhibition as the dominant mechanism (Bazzini et al., 2012). This suggests that, during early cleavage stages, miR-31 may interact with its targets dynamically, and without degrading the target mRNAs. Disruption of this process would lead to mitotic arrest, ultimately leading to embryonic lethality (Figs 6 and 7). We demonstrate for the first time that miR-31 regulates translation of its targets at the mitotic spindle and that disruption of this local regulation has a negative effect on early development (Figs 5 and 6). Overall, our results highlight the importance of miRNA-mediated post-transcriptional regulation at the spindles of the rapidly dividing early embryo, when efficient protein regulation is crucial, and indicate that this regulatory paradigm of mitosis may be evolutionarily conserved.

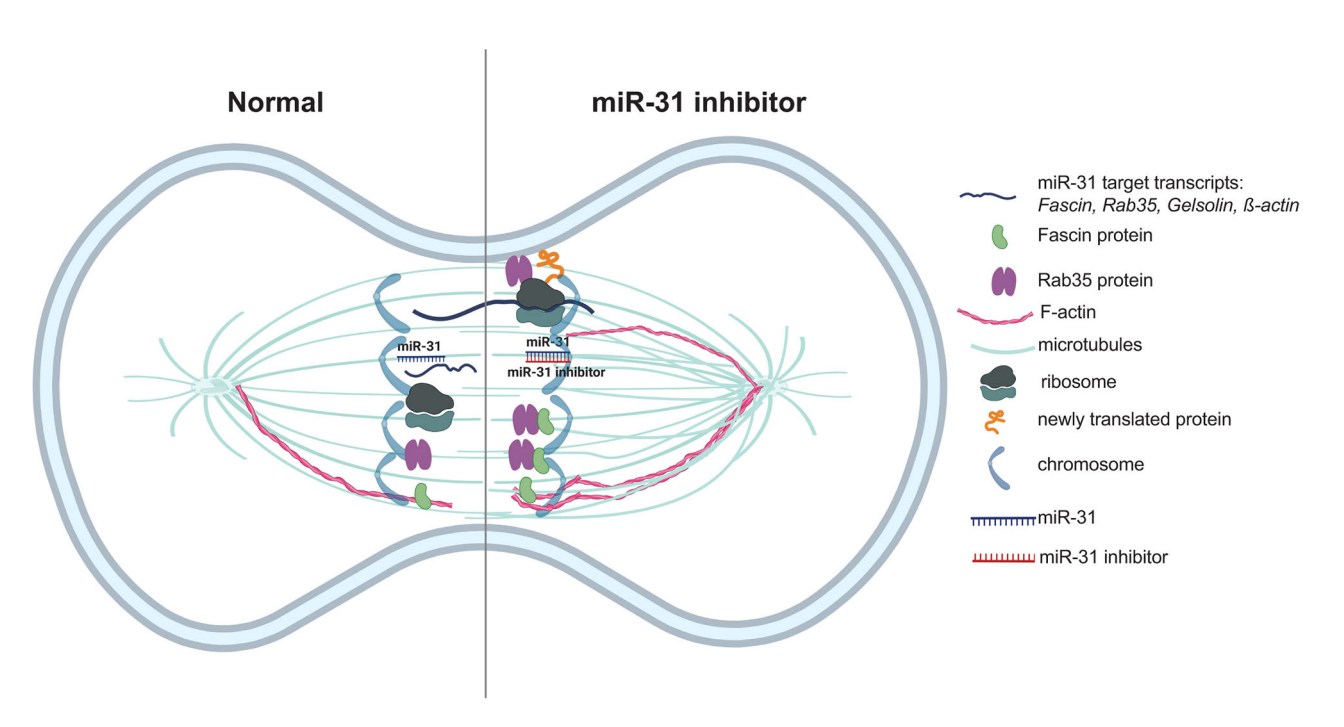


Fig. 7. Model of the regulation of local translation at the mitotic spindle by miR-31. miR-31 and its target transcripts localize to the mitotic spindle. miR-31 is hypothesized to dynamically regulate translation of its target transcripts such as β -actin, Gelsolin, Rab35 and Fascin to mediate local cytoskeletal dynamics in order to ensure proper mitotic progression. The left blastomere represents a normal cell; the right blastomere represents miR-31-inhibited cell. Created with BioRender.com

MATERIALS AND METHODS

Animals

Adult *Strongylocentrotus purpuratus* were collected from the California coast (Point Loma Marine Invertebrate Lab or Marinus Scientific). All animals and cultures were incubated at 12°C.

Microinjections

Microinjections were performed as previously described with modifications. Hsa-miR-31-3p Locked Nucleic Acid (LNA) power inhibitor (Qiagen) was resuspended with RNase-free water to $100 \,\mu\text{M}$. All sequences are listed in Table S3. Embryos were injected with $25 \,\mu\text{M}$ miR-31 LNA inhibitor, miRCURY LNA miRNA inhibitor negative control A or $25 \,\mu\text{M}$ control miR-124 LNA inhibitor, and collected at the 16- to 32-cell stage to phenotype for developmental defects. miR-124 is used as a negative control as it is not highly expressed in the early cleavage stage and is not enriched on the spindle. To test the importance of local translation of Fascin, we designed a translational blocking MASO (GeneTools) against Fascin. Fascin translational-blocking MASO, Fascin TP and control MASO (human β -globin) were resuspended with RNAse-free water to a 5 mM stock solution and diluted to 2 mM to perform microinjections. Rab35 TP was diluted to 1 mM for microinjections.

Injection solutions contained 20% sterile glycerol, 2 mg/ml 10,000 MW FITC lysine-charged dextran (Thermo Fisher Scientific), and miR-31 LNA power inhibitor, miR-124 LNA power inhibitor, control MASO or *Fascin* translational-blocking MASO. Injections were performed using the Pneumatic PicoPump with a vacuum (World Precision Instruments). A vertical needle puller PL-10 (Narishige International) was used to pull the injection needles (1 mm glass capillaries with filaments) (World Precision Instruments).

Biotinylated pull down with RNA seq

Embryos were injected with either Texas Red dye for controls or a biotinylated miR-31 mimic to identify potential targets (Tan and Lieberman, 2016). Potential miR-31 target transcripts pulled down by the biotinylated miR-31 mimic were validated with luciferase reporters with site-directed mutagenesis (please see the section 'Cloning of constructs for luciferase assays') as previously described (Stepicheva and Song, 2015). RNAs are sequenced with Illumina (50 bp single-end) and was assessed using FastQCv0.10.1 (https://www.bioinformatics.babraham.ac.uk/projects/fastqc/). Reads were trimmed for quality (Q<30) and analyzed using Trim Galore! v0.4.4 (https://www.bioinformatics.babraham.ac.uk/projects/trim_galore) with cutadapt v1.13 (Martin, 2011). Trimmed reads were aligned to the S. purpuratus genome (v3.1 with annotation build 8) housed in the Echinobase (Kudtarkar and Cameron, 2017) using TopHat2 v2.1.0 (Kim et al., 2013), mapping metrics were assessed using RseQC v2.6.1 (Wang et al., 2012) and gene/exon feature counts were calculated using HTseq v0.9.0 (Anders et al., 2015). Differential expression analysis was performed to identify gene-level features (CPM>1 in two or more samples) that were significantly up- or downregulated between miR-31 mimic-injected embryos and control embryos using a generalized linear model accounting for sample-to-sample variation in EdgeR v3.16.5 (Anders et al., 2013; Robinson et al., 2010) using the likelihood ratio test with FDR correction (q<0.05). To identify potential miR-31 binding sites in differentially expressed genes, BLAT (Kent et al., 2002) was used to identify potential miR-31 seed sequence ('TCTTGCC') matches within protein-coding genes allowing one mismatch.

Proteomics experiment

We conducted iTRAQ experiments to identify potential miR-31 targets. This approach allows us to examine simultaneously all the replicates of scrambled and miR-31-injected embryos by robust quantitative proteomics analysis to reduce variability. Two samples with four biological replicates were studied over two four-plex iTRAQ experiments. Proteomic sample preparation and data collection, starting with lysis (without calcium carbonate) through MSMS data processing was performed (Hou et al., 2013). Each sample containing 2000 injected embryos and 100 µg protein were subjected to protein reduction, alkylation and tryptic digestion. Digested samples underwent detergent removal and iTRAQ labeling; iTRAQ-labeled peptides were fractionated offline by high pH RP, then analyzed by low pH RP-ESI-MS/MS. Database searches were conducted

using Protein Pilot against the Echinobase database (Kudtarkar and Cameron, 2017). Only peptides with a confidence interval of at least 95% were selected for protein identification and quantification. ANOVA analysis was performed with JMP software as previously described (Hou et al., 2013). Proteins that had increased levels upon miR-31 inhibition compared with the control were analyzed bioinformatically. We took 1.5 kb of their 3′ UTRs and bioinformatically searched for the complement of the miR-31 seed sequence (Baek et al., 2008; Selbach et al., 2008).

RNA in situ hybridization

We performed fluorescence RNA in situ hybridization (FISH) as described previously with modifications (Sethi et al., 2014). Cel-miR-72 miRCURY LNA detection probes (Qiagen) were used to visualize miR-31 (Stepicheva and Song, 2015). To generate RNA probes against protein-coding transcripts for either the sea urchin or mammalian cell line FISH, PCR was used to amplify transcripts of interest from either sea urchin or LLC-PK cDNA. PCR primers used to make antisense probes are listed in Table S4. For double FISH, β-actin, Fascin, Rab35 and Gelsolin (DNP-labeled, MilliporeSigma) probes were co-incubated with miR-31 probe. All RNA probes were added at $0.5\;\text{ng/}\mu\text{l}$ and hybridized for 4-5 days, as described previously (Remsburg et al., 2023). All images were taken using the Zeiss LSM 880 scanning confocal microscope. The maximum intensity projections of z-stack images were acquired with Zen software and processed with Adobe Photoshop and Adobe Illustrator. FISH for LLC-PK (Hull et al., 1976) or HCT116 (Cekaite et al., 2012) were conducted as described previously (Martín-Durán et al., 2017) and incubated with 0.5 ng/µl DNP-labeled HsFascin probe and 0.1 ng/μl miR-31 miRCURY detection probe (Qiagen) at 50°C for 48 h.

Western blotting procedures

Three replicates of 150 cleavage stage embryos were injected with either control miR-124 LNA inhibitor or miR-31 LNA inhibitor. For Fascin and Rab35 antibody validation experiments, replicates of 150 cleavage stage embryos were injected with either control MASO or Fascin (five replicates), or Rab35 MASO (two replicates) (Fig. S2). HCT116 cells were cultured and resuspended in media to a concentration of 2×10⁶ cells/ml. Cells were spun at 13,548 g for 10 min at 4°C to pellet. Cells and embryos were lysed with RIPA buffer supplemented with protease inhibitor cocktail (MilliporeSigma) and suspended in homemade Laemmli Buffer with 5 mM DTT. Lysate was boiled at 100°C and spun down at 13,548 g for 10 min at 4°C. Samples were run on 12% SDS-PAGE gel and transferred onto nitrocellulose paper for 7 min using a semi dry transfer system (Bio-Rad) and semi-dry transfer buffer (48 mM Tris-Base, 39 mM glycine, 0.0375% SDS and 20% methanol). For the protein ladder, we used Magic Mark or precision plus protein standard (Bio-Rad). Blots were blocked for 1 h in 5% BSA in TBST (20 mM Tris-Base, 150 mM NaCl, 50 mM KCl and 0.2% Tween-20 at pH 7.6) and incubated in tubulin (E7 from Developmental Studies Hybridoma Bank) or pan-actin (JLA20 from Developmental Studies Hybridoma Bank), Fascin (1: 1000) or Rab35 (1:1000) antibodies (ProteinTech Group) in 5% BSA and TBST for 1 h at room temperature. After primary antibody incubation, blots were washed three times in TBST for 10 min on a rocker, and then incubated in rabbit-anti-mouse IgG HRP (MilliporeSigma) at 1:5000 in 5% BSA and TBST for 1 h. After three 10 min washes with TBST, blots were imaged on ChemiDoc machine (Bio-Rad). For detection of HA, Rab35 blot was stripped and incubated in monoclonal anti-HA antibody at a dilution of 1:5000 (ThermoFisher) in 5% BSA/TBST for 1 h, followed by three washes in TBST for 10 min on a rocker, and then incubated in 1:2500 rabbit-anti-mouse IgG HRP. Image J was used to quantify protein band intensities. Bands from control and miR-31 inhibitor or Fascin/Rab35 MASO-injected embryos were first normalized to the background and their arbitrary values were tabulated and averaged, and subjected to a paired Student's t-test for statistical analysis.

Immunolabeling procedures

To observe spatial localization of various proteins, immunolabeling was performed using antibodies against various cytoskeletal elements. E7 (anti- β -tubulin) (Developmental Studies Hybridoma Bank, E7, Lot 2/13/20-54 µg/ml) or anti- α -tubulin (11224-1-AP, ProteinTech Group) was used to label microtubules. Anti-Fascin (66321-1-lg, ProteinTech Group), anti-

Rab35 (11329-2-AP, ProteinTech Group) and anti-EEF1A1 (11402-1-AP, Proteintech) were used to label Fascin, Rab35 and EEF1A1, respectively. Embryos were fixed in 100% ice-cold methanol for 10 min on ice for immunolabeling for Fascin, 10% TCA in deionized $\rm H_2O$ for 30 min for immunolabeling for Rab35. Three 15 min phosphate-buffered saline 0.1% Triton (PBST) (10×PBS; Bio-Rad) washes were performed. Embryos were blocked with 4% sheep serum (MilliporeSigma) for 1 h at room temperature. Primary antibody incubation was performed with E7 at 1:10, Fascin and EEFA1 at 1:100, and Rab35 at 1:50, respectively. Embryos were washed three times for 15 min with PBST followed by incubation with the secondary antibodies goat anti-mouse (for E7 and Fascin) and goat antirabbit (α -tubulin and Rab35) Alexa 488 or Alexa 647 at 1:300 for 1 h at room temperature (Thermo Fisher Scientific), sequentially.

To examine F-actin, embryos were fixed to stabilize nuclear actin as previously described (Kita et al., 2019), then labeled with fluorescently conjugated phalloidin as previously described (Konrad and Song, 2022) with minor modifications. AlexaFluor-647 conjugated phalloidin (Thermo Fisher Scientific) was reconstituted in DMSO, then diluted to 10 U ml⁻¹ in PBST. Embryos were washed three times with PBST.

At least 10 embryos or cells were observed over at least three biological replicates. All immunolabeled embryos were counterstained with DAPI in PBST buffer (NucBlue; Thermo Fisher Scientific). All immunolabeled embryos were imaged using a Zeiss LSM 880 scanning confocal microscope using Zen software (Zeiss). The maximum intensity projections of *z*-stack images were acquired with Zen software and processed with Adobe Photoshop and Adobe Illustrator.

Cloning of constructs for luciferase assays

The miRNA prediction tools that perform best according to high-throughput validation all scan 3'UTRs for short motifs complementary to the miRNA seed sequences (Baek et al., 2008; Selbach et al., 2008). However, current miRNA prediction programs, such as PicTar and TargetScan rely heavily on conservation information, which is not yet available for the S. purpuratus genome. Therefore, the best tool we have now is to search for miRNA seed matches within 3'UTRs. We searched for 7/7 or 6/7 miR-31 seed matches within the 3'UTR of Fascin, Rab35, Actin and Gelsolin. Fascin has two miR-31 seed sequences. Both Rab35 and Gelsolin each have a single miR-31 seed site. β-Actin has seven seed sites, of which we mutated 3/7 to test. The 3'UTRs of Fascin and Gelsolin, and the CDS and 3'UTR of Rab35 and β-actin were cloned using sea urchin cDNA into pCR-Blunt vector (Table S4) (Thermo Fisher Scientific). Plasmids containing potential cloned DNA inserts were subjected to DNA sequencing (Genewiz Services). These were subcloned downstream of the Renilla luciferase (RLuc) as described previously. The miR-31 binding sites within Fascin, *Rab35*, *Gelsolin* and β -actin were mutagenized at the third and fifth binding sites by using the QuikChange Lightning Kit (Agilent Technologies). The sequence of the mutagenesis primers used is listed in Table S4. Clones were sequenced to check for the mutated miR-31 binding site (Genewiz Services). Firefly construct (FF) was linearized using SpeI and in vitro transcribed with SP6 RNA polymerase. Transcripts were purified using the RNA Nucleospin Clean-up kit (Macherey-Nagel). FF and reporter RLuc constructs were co-injected at 50 ng/µl. Fifty embryos at the mesenchyme blastula stage (24 hpf) were collected in 25 μl of 1×Promega passive lysis buffer and vortexed at room temperature. Dual-luciferase assays were performed using the Promega Dual-Luciferase Reporter (DLR) Assay Systems with the Promega GloMax 20/20 Luminometry System (Promega). The rest of the assay was performed as previously described (Stepicheva and Song, 2015).

Puro-PLA assay

To detect newly translated Fascin, we used the Puro-PLA assay using the DuoLink PLA kit (MilliporeSigma). Experiments in the HCT116 cells were performed as described previously (Chin and Lécuyer, 2021) with minor modifications. Cells were incubated overnight on coverslips, then incubated for 30 min in cycloheximide or cell culture media, then incubated in either cycloheximide and 2 μM puromycin, 2 μM puromycin alone or 0.002% DMSO (solvent negative control). Cells were washed with PBS-MC (PBS, 1 mM MgCl₂ and 0.1 mM CaCl₂), then fixed with 4% PFA and 4% sucrose

in PBS-MC. Cells were incubated in mouse anti-Fascin antibody (ECM Biosciences, FM2651) at 1:100 and rabbit anti-puromycin antibody (AbClonal A23031) at 1:1000. After rolling circle amplification step, cells were incubated in Alexa-488 conjugated anti-tubulin antibody at 1:100 (Thermo Fisher Scientific) overnight. Experiments in embryos were performed as described above, with the following modifications: cycloheximide was used at 20 μ M and puromycin was used at 50 μ g/ml. Embryos were fixed in 4% PFA in filtered sea water for 1 h at room temperature. The puromycin antibody was used at 1:100. Embryos were counterstained with NucBlue (Thermo Fisher Scientific).

ImageJ analysis

To quantitatively analyze the change in tubulin, actin, Fascin and Rab35 observed after miR-31 inhibition, single plane confocal images of blastomeres were exported from Zen as TIFFs. For tubulin and F-actin level measurements, signals within entire anaphase blastomeres were quantified. For Fascin and Rab35 subcellular localization to the spindles, we selected a single slice of the z-stack that corresponded to the center of the spindle that had both sets of chromosomes visible. We then selected the region of the spindle as a region of interest (ROI), determined the mean fluorescence intensity (mean gray value) using ImageJ (Schneider et al., 2012). These were graphed and a Student's t-test was used to test for statistical significance. To quantify newly translated Fascin protein after miR-31 inhibition (Fig. 5A), a maximum intensity projection of five 1 μm thick slices was created in Zen and exported as a TIFF. The numbers of fluorescent dots, which are indicative of newly synthesized Fascin, were counted in the mitotic spindle area and in the cytoplasmic area, excluding the mitotic spindle. The numbers of dots were then divided by the area to determine the density of newly translated Fascin in each region. The mean density of Fascin at the spindle and the cytoplasm for each replicate was calculated, and the means were used to test for significant differences between control and miR-31-inhibited embryos using an unpaired, two-tailed Student's t-test to calculate the significance between control and miR-31-inhibited embryos.

To quantify F-actin and tubulin (Fig. 1F,G), we also performed line scans. Single slice z-stacks were exported from Zen as TIFFs and opened in ImageJ. A line with a pixel width of 1 was drawn across the diameter of the blastomere, running parallel to the axis of cell division. The axis of division was determined by the orientation of the chromosomes from DAPI stain. Fluorescence intensity was measured at each pixel along the line. The data were then normalized to a length of 50 points, by averaging equally sized groups along the x-axis. For example, if the blastomere was 300 pixels long, the fluorescence intensities for sequential six groups of pixels were averaged. This allowed us to normalize for blastomere length. After normalizing for length, the fluorescence intensity was averaged for each replicate at each point along the line. These data were then plotted as average fluorescent intensity across the diameter of the blastomere.

Preparation of RNA transcripts for injections

To understand the role that localized translation plays in development, we used the PP7-coat protein and the PP7 RNA motifs previously used to localize and visualize RNA transcripts (Yan et al., 2016). We sub-cloned 24 repeats of the PP7 motif (obtained from Addgene 74928) into the pCR-Blunt vector. We cloned the CDS of Fascin from cDNA into pCR-Blunt vector (Thermo Fisher Scientific), then sub-cloned the Fascin CDS into the PP7 motif containing vector. We also synthesized the Fascin CDS+3'UTR (Twist Biosciences). These plasmids were linearized with the appropriate restriction enzymes and transcribed using mMessage mMachine kit (Thermo Fisher Scientific), purified using the RNA Nucleospin Clean-up kit (Macherey-Nagel) and filtered through a Millipore UltraFree 0.22µm filter. Transcripts were injected at 1 $\mu g/\mu l$.

Purification of PP7-mCherry-CAAX

pHR-PP7-2xmCherry-CAAX plasmid (Addgene 74925) was subcloned into the pNOTAT vector and transformed into NiCO (DE3) cells (MilliporeSigma). Protein expression was induced with 1 mM IPTG (Thermo Fisher Scientific) at 30°C. Protein was purified using Ni-NTA Fast Start kit (Qiagen) and dialyzed in dialysis buffer (136 mM NaCl, 2.7 mM KCl, 10 mM Na₂HPO₄,

 $1.7~mM\ NaH_2PO_4,\ 10\%$ glycerol and $0.1~mM\ DTT$ at pH 7.0). Protein was aliquoted and stored at $-80^{\circ}C$ until used for microinjections.

Preadsorption study to test the specificity of the Rab35 antibody

The specificity of the Rab35 antibody was tested with a preadsorption assay. The sea urchin Rab35 CDS is cloned into a HA and 6x-poly histidine pNOTAT expression vector, and transformed into C41 cells (Lucigen). Bacterial lysates expressing Rab35-HA-HIS were used to conduct preadsorption tests. The Rab35 antibody was preadsorbed in blocking buffer (PBST-0.1% Triton in 4% sheep serum) with bacterial lysate expressing the sea urchin Rab35 protein or bacterial lysate transformed with the empty pNOTAT vector coated on PVDF membranes (BioRad) in Eppendorf tubes overnight at 4°C. Rab35 antibody preadsorbed with bacterial lysate with or without Rab35 was used in immunolabeling experiments (Fig. S2C). See the supplementary Materials and Methods for more details.

Statistical analysis

Statistical tests used were Cochran-Mantel-Haenszel tests, Fisher's exact, ANOVA with a Tukey-Kramer post-hoc test or a Student's *t*-test. Two-tailed Student's *t*-tests were performed in all cases, except when specified as one-tailed. Mean values were calculated for each replicate, then an unpaired, two-tailed *t*-test was performed using the means of each replicate.

Acknowledgements

We thank members of our laboratory for their comments. We thank Dr. Shuo Wei (University of Delaware) for the HCT116 cells and Dr. Gary Laverty (University of Delaware) for the LLC-PK cells. We thank Dr. Ramona Neunuebel for the human Rab35 construct. Some of the text and figures in this paper formed part of Carolyn Remsburg's PhD dissertation in the Department of Biological Sciences at the University of Delaware in 2023. Access to the Bioimaging core facility was supported by the Institutional Development Award (IDeA) from the National Institute of Health's National Institute of General Medical Sciences (P20GM103446).

Competing interests

The authors declare no competing or financial interests.

Author contributions

Conceptualization: C.M.R., K.D.K., J.L.S.; Methodology: C.M.R., K.D.K., M.D.T., N.S., K.L., L.L.C., S.P., J.B., H.H., J.L.S.; Validation: C.M.R., K.D.K., M.D.T., L.L.C.; Formal analysis: C.M.R., K.D.K., J.B., J.L.S.; Investigation: K.D.K., J.L.S.; Resources: K.L., S.P., J.L.S.; Data curation: C.M.R., K.D.K.; Writing - original draft: C.M.R.; Writing - review & editing: C.M.R., J.L.S.; Visualization: K.D.K., N.S., J.L.S.; Supervision: J.L.S.; Project administration: C.M.R., K.D.K., M.D.T., N.S., K.L., L.L.C., S.P., J.B., H.H., J.L.S.; Funding acquisition: J.L.S.

Funding

This work is funded by the National Science Foundation (IOS 1553338 and MCB 2103453 to J.L.S.), the National Institutes of Health (P20GM103653 and P20GM103446), Delaware IDeA Network of Biomedical Research Excellence (P20GM103446) and Sigma Xi Grants-in-Aid of Research (20A01418 to C.M.R.). Deposited in PMC for release after 12 months.

Data availability

The data that support the findings of this study are available from the corresponding author upon request.

The people behind the papers

This article has an associated 'The people behind the papers' interview with some of the authors.

References

- Addi, C., Bai, J. and Echard, A. (2018). Actin, microtubule, septin and ESCRT filament remodeling during late steps of cytokinesis. *Curr. Opin. Cell Biol.* 50, 27-34. doi:10.1016/j.ceb.2018.01.007
- Addi, C., Presle, A., Frémont, S., Cuvelier, F., Rocancourt, M., Milin, F., Schmutz, S., Chamot-Rooke, J., Douché, T., Duchateau, M. et al. (2020). The Flemmingsome reveals an ESCRT-to-membrane coupling via ALIX/syntenin/syndecan-4 required for completion of cytokinesis. *Nat. Commun.* 11, 1941. doi:10.1038/s41467-020-15205-z
- Anders, S., Mccarthy, D. J., Chen, Y., Okoniewski, M., Smyth, G. K., Huber, W. and Robinson, M. D. (2013). Count-based differential expression analysis of

- RNA sequencing data using R and Bioconductor. *Nat. Protoc.* **8**, 1765-1786. doi:10.1038/nprot.2013.099
- Anders, S., Pyl, P. T. and Huber, W. (2015). HTSeq–a Python framework to work with high-throughput sequencing data. *Bioinformatics* 31, 166-169. doi:10.1093/bioinformatics/btu638
- Baek, D., Villén, J., Shin, C., Camargo, F. D., Gygi, S. P. and Bartel, D. P. (2008). The impact of microRNAs on protein output. *Nature* 455, 64-71. doi:10.1038/nature07242
- Bartel, D. P. (2018). Metazoan MicroRNAs. Cell 173, 20-51. doi:10.1016/j.cell.2018. 03.006
- Batty, P. and Gerlich, D. W. (2019). Mitotic chromosome mechanics: how cells segregate their genome. *Trends Cell Biol.* **29**, 717-726. doi:10.1016/j.tcb.2019.05.
- Bazzini, A. A., Lee, M. T. and Giraldez, A. J. (2012). Ribosome profiling shows that miR-430 reduces translation before causing mRNA decay in zebrafish. *Science* 336, 233-237. doi:10.1126/science.1215704
- Blower, M. D., Feric, E., Weis, K. and Heald, R. (2007). Genome-wide analysis demonstrates conserved localization of messenger RNAs to mitotic microtubules. *J. Cell Biol.* **179**, 1365-1373. doi:10.1083/jcb.200705163
- Booth, A. J. R., Yue, Z., Eykelenboom, J. K., Stiff, T., Luxton, G. G. W., Hochegger, H. and Tanaka, T. U. (2019). Contractile acto-myosin network on nuclear envelope remnants positions human chromosomes for mitosis. *eLife* 8, e46902. doi:10.7554/eLife.46902
- Cao, J., Crest, J., Fasulo, B. and Sullivan, W. (2010). Cortical actin dynamics facilitate early-stage centrosome separation. *Curr. Biol.* 20, 770-776. doi:10.1016/ j.cub.2010.02.060
- Capalbo, L., Bassi, Z. I., Geymonat, M., Todesca, S., Copoiu, L., Enright, A. J., Callaini, G., Riparbelli, M. G., Yu, L., Choudhary, J. S. et al. (2019). The midbody interactome reveals unexpected roles for PP1 phosphatases in cytokinesis. *Nat. Commun.* 10, 4513. doi:10.1038/s41467-019-12507-9
- Cekaite, L., Rantala, J. K., Bruun, J., Guriby, M., Ågesen, T. H., Danielsen, S. A., Lind, G. E., Nesbakken, A., Kallioniemi, O., Lothe, R. A. et al. (2012). MiR-9, -31, and -182 deregulation promote proliferation and tumor cell survival in colon cancer. *Neoplasia* 14, 868-879. doi:10.1593/neo.121094
- Chassé, H., Mulner-Lorillon, O., Boulben, S., Glippa, V., Morales, J. and Cormier, P. (2016). Cyclin B translation depends on mTOR activity after fertilization in sea urchin embryos. *PLoS ONE* 11, e0150318. doi:10.1371/journal.pone.0150318
- Chassé, H., Boulben, S., Cormier, P. and Morales, J. (2019). Translational control of canonical and non-canonical translation initiation factors at the sea urchin egg to embryo transition. *Int. J. Mol. Sci.* 20, 626. doi:10.3390/ijms20030626
- Chesneau, L., Dambournet, D., Machicoane, M., Kouranti, I., Fukuda, M., Goud, B. and Echard, A. (2012). An ARF6/Rab35 GTPase cascade for endocytic recycling and successful cytokinesis. *Curr. Biol.* 22, 147-153. doi:10.1016/j.cub. 2011.11.058
- Chin, A. and Lécuyer, E. (2021). Puromycin labeling coupled with proximity ligation assays to define sites of mRNA translation in Drosophila embryos and human cells. *Methods Mol. Biol.* **2381**, 267-284. doi:10.1007/978-1-0716-1740-3_15
- Colin, A., Singaravelu, P., Théry, M., Blanchoin, L. and Gueroui, Z. (2018). Actinnetwork architecture regulates microtubule dynamics. *Curr. Biol.* 28, 2647-2656.e4. doi:10.1016/j.cub.2018.06.028
- Crist, C. G., Montarras, D. and Buckingham, M. (2012). Muscle satellite cells are primed for myogenesis but maintain quiescence with sequestration of Myf5 mRNA targeted by microRNA-31 in mRNP granules. Cell Stem Cell 11, 118-126. doi:10. 1016/j.stem.2012.03.011
- Farmer, T., Vaeth, K. F., Han, K.-J., Goering, R., Taliaferro, M. J. and Prekeris, R. (2023). The role of midbody-associated mRNAs in regulating abscission. J. Cell Biol. 222, e202306123. doi:10.1083/jcb.202306123
- Feldt, J., Schicht, M., Garreis, F., Welss, J., Schneider, U. W. and Paulsen, F. (2019). Structure, regulation and related diseases of the actin-binding protein gelsolin. Expert Rev. Mol. Med. 20, e7. doi:10.1017/erm.2018.7
- Fernandez-Nicolas, A., Uchida, A., Poon, J. and Yajima, M. (2022). Vasa nucleates asymmetric translation along the mitotic spindle during unequal cell divisions. *Nat. Commun.* 13, 2145. doi:10.1038/s41467-022-29855-8
- Ge, F., Wang, C., Wang, W., Liu, W. and Wu, B. (2017). MicroRNA-31 inhibits tumor invasion and metastasis by targeting RhoA in human gastric cancer. *Oncol. Rep.* 38, 1133-1139. doi:10.3892/or.2017.5758
- Groisman, I., Huang, Y.-S., Mendez, R., Cao, Q., Theurkauf, W. and Richter, J. D. (2000). Cpeb, maskin, and cyclin B1 mRNA at the mitotic apparatus: implications for local translational control of cell division. *Cell* 103, 435-447. doi:10.1016/S0092-8674(00)00135-5
- Hassine, S., Bonnet-Magnaval, F., BENOIT Bouvrette, L. P., Doran, B., Ghram, M., Bouthillette, M., Lecuyer, E. and Desgroseillers, L. (2020). Staufen1 localizes to the mitotic spindle and controls the localization of RNA populations to the spindle. *J. Cell Sci.* 133, jcs247155. doi:10.1242/jcs.247155
- Heinz, L. S., Muhs, S., Schiewek, J., Grüb, S., Nalaskowski, M., Lin, Y.-N., Wikman, H., Oliveira-Ferrer, L., Lange, T., Wellbrock, J. et al. (2017). Strong fascin expression promotes metastasis independent of its F-actin bundling activity. Oncotarget 8, 110077-110091. doi:10.18632/oncotarget.22249

- Hou, S., Jones, S. W., Choe, L. H., Papoutsakis, E. T. and Lee, K. H. (2013). Workflow for quantitative proteomic analysis of Clostridium acetobutylicum ATCC 824 using iTRAQ tags. *Methods* 61, 269-276. doi:10.1016/j.ymeth.2013.03.013
- Hsieh, C. H. and Wang, Y. C. (2022). Emerging roles of plasma gelsolin in tumorigenesis and modulating the tumor microenvironment. *Kaohsiung J. Med.* Sci. 38, 819-825. doi:10.1002/kjm2.12578
- Hull, R. N., Cherry, W. R. and Weaver, G. W. (1976). The origin and characteristics of a pig kidney cell strain, LLC-PK. In vitro 12, 670-677. doi:10.1007/BF02797469
- Imami, K., Milek, M., Bogdanow, B., Yasuda, T., Kastelic, N., Zauber, H., Ishihama, Y., Landthaler, M. and Selbach, M. (2018). Phosphorylation of the ribosomal protein RPL12/uL11 affects translation during mitosis. *Mol. Cell* 72, 84-98.e9. doi:10.1016/j.molcel.2018.08.019
- Jayo, A. and Parsons, M. (2010). Fascin: a key regulator of cytoskeletal dynamics. Int. J. Biochem. Cell Biol. 42, 1614-1617. doi:10.1016/j.biocel.2010.06.019
- Jewett, C. E., Vanderleest, T. E., Miao, H., Xie, Y., Madhu, R., Loerke, D. and Blankenship, J. T. (2017). Planar polarized Rab35 functions as an oscillatory ratchet during cell intercalation in the Drosophila epithelium. *Nat. Commun.* 8, 476. doi:10.1038/s41467-017-00553-0
- Kelpsch, D. J., Groen, C. M., Fagan, T. N., Sudhir, S. and Tootle, T. L. (2016). Fascin regulates nuclear actin during *Drosophila* oogenesis. *Mol. Biol. Cell* 27, 2965-2979. doi:10.1091/mbc.E15-09-0634
- Kent, W. J., Sugnet, C. W., Furey, T. S., Roskin, K. M., Pringle, T. H., Zahler, A. M. and Haussler, D. (2002). The human genome browser at UCSC. *Genome Res.* 12, 996-1006. doi:10.1101/gr.229102
- Kim, D., Pertea, G., Trapnell, C., Pimentel, H., Kelley, R. and Salzberg, S. L. (2013). TopHat2: accurate alignment of transcriptomes in the presence of insertions, deletions and gene fusions. *Genome Biol.* 14, R36. doi:10.1186/gb-2013-14-4-r36
- Kita, A. M., Swider, Z. T., Erofeev, I., Halloran, M. C., Goryachev, A. B. and Bement, W. M. (2019). Spindle-F-actin interactions in mitotic spindles in an intact vertebrate epithelium. *Mol. Biol. Cell* 30, 1645-1654. doi:10.1091/mbc.E19-02-0126
- Klinkert, K., Rocancourt, M., Houdusse, A. and Echard, A. (2016). Rab35 GTPase couples cell division with initiation of epithelial apico-basal polarity and lumen opening. *Nat. Commun.* 7, 11166-11166. doi:10.1038/ncomms11166
- Konrad, K. D. and Song, J. L. (2022). microRNA-124 regulates Notch and NeuroD1 to mediate transition states of neuronal development. *Dev. Neurobiol.* 83, 3-27. doi:10.1101/2021.12.10.471989
- Konrad, K. D., Arnott, M., Testa, M., Suarez, S. and Song, J. L. (2023). microRNA-124 directly suppresses Nodal and Notch to regulate mesodermal development. Dev. Biol. 502, 50-62. doi:10.1016/j.ydbio.2023.06.017
- Kudtarkar, P. and Cameron, R. A. (2017). Echinobase: an expanding resource for echinoderm genomic information. *Database (Oxford)* 2017, bax074. doi:10.1093/ database/bax074
- Lanni, J. S. and Jacks, T. (1998). Characterization of the p53-dependent postmitotic checkpoint following spindle disruption. *Mol. Cell. Biol.* 18, 1055-1064. doi:10.1128/MCB.18.2.1055
- Lawson, C. D., Peel, S., Jayo, A., Corrigan, A., Iyer, P., BAXTER Dalrymple, M., Marsh, R. J., Cox, S., VAN Audenhove, I., Gettemans, J. et al. (2022). Nuclear fascin regulates cancer cell survival. eLife 11, e79283. doi:10.7554/eLife.79283
- Lenk, R., Ransom, L., Kaufmann, Y. and Penman, S. (1977). A cytoskeletal structure with associated polyribosomes obtained from HeLa cells. Cell 10, 67-78. doi:10.1016/0092-8674(77)90141-6
- Lin, Z., Gasic, I., Chandrasekaran, V., Peters, N., Shao, S., Mitchison, T. J. and Hegde, R. S. (2020). TTC5 mediates autoregulation of tubulin via mRNA degradation. *Science* 367, 100-104. doi:10.1126/science.aaz4352
- Lv, C., Li, F., Li, X., Tian, Y., Zhang, Y., Sheng, X., Song, Y., Meng, Q., Yuan, S., Luan, L. et al. (2017). MiR-31 promotes mammary stem cell expansion and breast tumorigenesis by suppressing Wnt signaling antagonists. *Nat. Commun.* 8, 1036. doi:10.1038/s41467-017-01059-5
- Martin, M. (2011). Cutadapt removes adapter sequences from high-throughput sequencing reads. EMBnet. J. 17, 10. doi:10.14806/ej.17.1.200
- Martín-Durán, J. M., Passamaneck, Y. J., Martindale, M. Q. and Hejnol, A. (2017). The developmental basis for the recurrent evolution of deuterostomy and protostomy. *Nat. Ecol. Evol.* 1, 0005. doi:10.1038/s41559-016-0005
- McIntosh, J. R. (2016). Mitosis. Cold Spring Harbor Perspect. Biol. 8, a023218. doi:10.1101/cshperspect.a023218
- Mizoguchi, F., Murakami, Y., Saito, T., Miyasaka, N. and Kohsaka, H. (2013). miR-31 controls osteoclast formation and bone resorption by targeting RhoA. Arthritis Res. Ther. 15, R102. doi:10.1186/ar4282
- Orth, J. D., Loewer, A., Lahav, G. and Mitchison, T. J. (2012). Prolonged mitotic arrest triggers partial activation of apoptosis, resulting in DNA damage and p53 induction. *Mol. Biol. Cell* 23, 567-576. doi:10.1091/mbc.e11-09-0781
- Otto, J. J., Kane, R. E. and Bryan, J. (1980). Redistribution of actin and fascin in sea urchin eggs after fertilization. *Cell Motil.* 1, 31-40. doi:10.1002/cm.970010104
- Park, S., Dahn, R., Kurt, E., Presle, A., Vandenheuvel, K., Moravec, C., Jambhekar, A., Olukoga, O., Shepherd, J., Echard, A. et al. (2023). The mammalian midbody and midbody remnant are assembly sites for RNA and localized translation. *Dev. Cell* 58, 1917-1932.e6. doi:10.1016/j.devcel.2023.07. 009

- Pascual, R., Segura-Morales, C., Omerzu, M., Bellora, N., Belloc, E., Castellazzi, C. L., Reina, O., Eyras, E., Maurice, M. M., Millanes-Romero, A. et al. (2021). mRNA spindle localization and mitotic translational regulation by CPEB1 and CPEB4. RNA 27, 291-302. doi:10.1261/rna.077552.120
- Peterman, E. and Prekeris, R. (2019). The postmitotic midbody: Regulating polarity, stemness, and proliferation. J. Cell Biol. 218, 3903-3911. doi:10.1083/jcb. 201906148
- Peterman, E., Gibieža, P., Schafer, J., Skeberdis, V. A., Kaupinis, A., Valius, M., Heiligenstein, X., Hurbain, I., Raposo, G. and Prekeris, R. (2019). The post-abscission midbody is an intracellular signaling organelle that regulates cell proliferation. *Nat. Commun.* 10, 3181. doi:10.1038/s41467-019-10871-0
- Petsalaki, E. and Zachos, G. (2021). The abscission checkpoint: a guardian of chromosomal stability. *Cells* 10, 3350. doi:10.3390/cells10123350
- Pollard, T. D. (2016). Actin and actin-binding proteins. Cold Spring Harbor Perspect. Biol. 8, a018226. doi:10.1101/cshperspect.a018226
- Prosser, S. L. and Pelletier, L. (2017). Mitotic spindle assembly in animal cells: a fine balancing act. Nat. Rev. Mol. Cell Biol. 18, 187-201. doi:10.1038/nrm.2016.162
- Rai, A., Greening, D. W., Xu, R., Chen, M., Suwakulsiri, W. and Simpson, R. J. (2021). Secreted midbody remnants are a class of extracellular vesicles molecularly distinct from exosomes and microparticles. *Commun. Biol.* 4, 400. doi:10.1038/s42003-021-01882-z
- Remsburg, C., Konrad, K., Sampilo, N. F. and Song, J. L. (2019). Analysis of microRNA functions. *Methods Cell Biol.* 151, 323-344. doi:10.1016/bs.mcb.2018. 10.005
- Remsburg, C., Testa, M. and Song, J. L. (2021). Rab35 regulates skeletogenesis and gastrulation by facilitating actin remodeling and vesicular trafficking. *Cells Dev.* 165, 203660-203660. doi:10.1016/j.cdev.2021.203660
- Remsburg, C. M., Konrad, K. D. and Song, J. L. (2023). RNA localization to the mitotic spindle is essential for early development and is regulated by kinesin-1 and dynein. J. Cell Sci. 136, jcs260528. doi:10.1242/jcs.260528
- Robinson, M. D., Mccarthy, D. J. and Smyth, G. K. (2010). edgeR: a Bioconductor package for differential expression analysis of digital gene expression data. *Bioinformatics* 26, 139-140. doi:10.1093/bioinformatics/btp616
- Sampilo, N. F., Stepicheva, N. A. and Song, J. L. (2021). microRNA-31 regulates skeletogenesis by direct suppression of Eve and Wnt1. Dev. Biol. 472, 98-114. doi:10.1016/j.ydbio.2021.01.008
- Santaguida, S. and Amon, A. (2015). Short- and long-term effects of chromosome mis-segregation and aneuploidy. *Nat. Rev. Mol. Cell Biol.* 16, 473-485. doi:10. 1038/nrm4025
- Schneider, C. A., Rasband, W. S. and Eliceiri, K. W. (2012). NIH Image to ImageJ: 25 years of image analysis. *Nat. Methods* **9**, 671-675. doi:10.1038/nmeth.2089
- Selbach, M., Schwanhäusser, B., Thierfelder, N., Fang, Z., Khanin, R. and Rajewsky, N. (2008). Widespread changes in protein synthesis induced by microRNAs. *Nature* 455, 58-63. doi:10.1038/nature07228
- Sethi, A. J., Angerer, R. C. and Angerer, L. M. (2014). Multicolor labeling in developmental gene regulatory network analysis. *Methods Mol. Biol.* 1128, 249-262. doi:10.1007/978-1-62703-974-1_17
- Siefert, J. C., Clowdus, E. A. and Sansam, C. L. (2015). Cell cycle control in the early embryonic development of aquatic animal species. *Comp. Biochem. Physiol. C Toxicol. Pharmacol.* 178, 8-15. doi:10.1016/j.cbpc.2015.10.003
- Skop, A. R., Liu, H., Yates, J., III, Meyer, B. J. and Heald, R. (2004). Dissection of the mammalian midbody proteome reveals conserved cytokinesis mechanisms. *Science* 305, 61-66. doi:10.1126/science.1097931
- Staton, A. A. and Giraldez, A. J. (2011). Use of target protector morpholinos to analyze the physiological roles of specific miRNA-mRNA pairs in vivo. *Nat. Protoc.* 6, 2035-2049. doi:10.1038/nprot.2011.423
- Stepicheva, N. A. and Song, J. L. (2015). microRNA-31 modulates skeletal patterning in the sea urchin embryo. *Development* 142, 3769-3780. doi:10.1242/ dev.127969
- Stonyte, V., Boye, E. and Grallert, B. (2018). Regulation of global translation during the cell cycle. *J. Cell Sci.* 131, jcs220327. doi:10.1242/jcs.220327
- Su, Y., Yu, Y., Liu, C., Zhang, Y., Liu, C., Ge, M., Li, L., Lan, M., Wang, T., Li, M. et al. (2020). Fate decision of satellite cell differentiation and self-renewal by miR-31-IL34 axis. *Cell Death Differ*. **27**, 949-965. doi:10.1038/s41418-019-0390-x
- Tan, S. M. and Lieberman, J. (2016). Capture and Identification of miRNA Targets by Biotin Pulldown and RNA-seq. *Methods Mol. Biol.* 1358, 211-228. doi:10.1007/ 978-1-4939-3067-8_13
- Tanenbaum, M. E., Stern-Ginossar, N., Weissman, J. S. and Vale, R. D. (2015).
 Regulation of mRNA translation during mitosis. *eLife* 4, e07957. doi:10.7554/eLife.07957
- **Testa, M., Remsburg, C. and Song, J. L.** (2023). The actin bundling protein Fascin is important for proper early development in Strongylocentrotus purpuratus embryos. *microPubl. Biol.* doi:10.17912/micropub.biology.000717
- Tian, Y., Ma, X., Lv, C., Sheng, X., Li, X., Zhao, R., Song, Y., Andl, T., Plikus, M. V., Sun, J. et al. (2017). Stress responsive miR-31 is a major modulator of mouse intestinal stem cells during regeneration and tumorigenesis. *eLife* 6, e29538. doi:10.7554/eLife.29538
- Villari, G., Jayo, A., Zanet, J., Fitch, B., Serrels, B., Frame, M., Stramer, B. M., Goult, B. T. and Parsons, M. (2015). A direct interaction between fascin and

- microtubules contributes to adhesion dynamics and cell migration. *J. Cell Sci.* **128**, 4601-4614. doi:10.1242/jcs.175760
- Waldron, A. and Yajima, M. (2020). Localized translation on the mitotic apparatus: a history and perspective. *Dev. Biol.* 468, 55-58. doi:10.1016/j.ydbio. 2020.09.010
- Wang, L., Wang, S. and Li, W. (2012). RSeQC: quality control of RNA-seq experiments. *Bioinformatics* 28, 2184-2185. doi:10.1093/bioinformatics/bts356
- Yan, X., Hoek, T. A., Vale, R. D. and Tanenbaum, M. E. (2016). Dynamics of translation of single mRNA molecules in vivo. *Cell* 165, 976-989. doi:10.1016/j. cell.2016.04.034
- Yu, H., Yang, F., Dong, P., Liao, S., Liu, W. R., Zhao, G., Qin, B., Dou, Z., Liu, Z., Liu, W. et al. (2019). NDP52 tunes cortical actin interaction with astral microtubules

- for accurate spindle orientation. *Cell Res.* **29**, 666-679. doi:10.1038/s41422-019-0189-9
- Zanet, J., Jayo, A., Plaza, S., Millard, T., Parsons, M. and Stramer, B. (2012).
 Fascin promotes filopodia formation independent of its role in actin bundling.
 J. Cell Biol. 197, 477-486. doi:10.1083/jcb.201110135
- Zhang, J., Fonovic, M., Suyama, K., Bogyo, M. and Scott, M. P. (2009). Rab35 Controls Actin Bundling by Recruiting Fascin as an Effector Protein. *Science* 325, 1250-1254. doi:10.1126/science.1174921
- Zheng, J., Zhou, H., Yang, T., Liu, J., Qin, T., Gu, X., Wu, J., Zhang, Y., Wang, H., Tang, Y. et al. (2021). Protective role of microRNA-31 in acetaminophen-induced liver injury: a negative regulator of c-Jun N-Terminal Kinase (JNK) signaling pathway. *Cell. Mol. Gastroenterol. Hepatol.* 12, 1789-1807. doi:10.1016/j.jcmgh.2021.07.011

Supplementary Materials and Methods

Preadsorption assay

Sea urchin Rab35 CDS was cloned upstream of a pNOTAT expression vector with HA and 6x HIS (Nagahara et al., 1998). The expected size of sea urchin Rab35 with the HIS and HA tag is a ~29 kDa protein. Sea urchin Rab35-HA-HIS was transformed into C41 competent cells (Lucigen, Middleton, WI). For negative control, C41 competent cells were transformed with the pNOTAT plasmid. All transformed cells were induced with 1mM IPTG for protein expression at 30°C for 5 h. 5mL of bacterial culture was spun down and lysed with RIPA buffer supplemented with protease inhibitor cocktail (MilliporeSigma, St. Louis, MO), and spun down at 12,000 rpm for 10 min at 4°C. Supernatant was collected from bacteria expressing the sea urchin Rab35 or the pNOTAT plasmid and coated on nitrocellulose 0.5 cm x 0.5 cm membrane (BioRad, Philadelphia, PA). The Rab35 antibody (1:50) was incubated with these membranes and pre-adsorbed in blocking buffer (PBST- 0.1% Triton in 4% sheep serum) for 5 h at 4°C. Rab35 antibody was then used to immunolabel cleavage stage sea urchin embryos overnight at 4C. Embryos were washed with PBST and incubated with goat anti-rabbit Alexa 647 in blocking buffer for 1 h at RT and counterstained with DAPI. Single slice images were acquired with Zeiss LSM 880 scanning confocal microscope (Carl Zeiss Incorporation, White Plains, NY). Non-dividing blastomeres were imaged at +/- 4 µm from the equatorial midpoint (with the highest fluorescent intensity for DAPI) and compiled as projected images. These images were exported from Zen as a TIFF (Tag Image File Format) and analyzed in ImageJ (Schneider et al., 2012). A region spanning the area of each blastomere was selected and the mean fluorescence intensity (MFI) was measured. Background signal taken from the outside of the embryo was subtracted from the fluorescent reading within the blastomere for normalization.

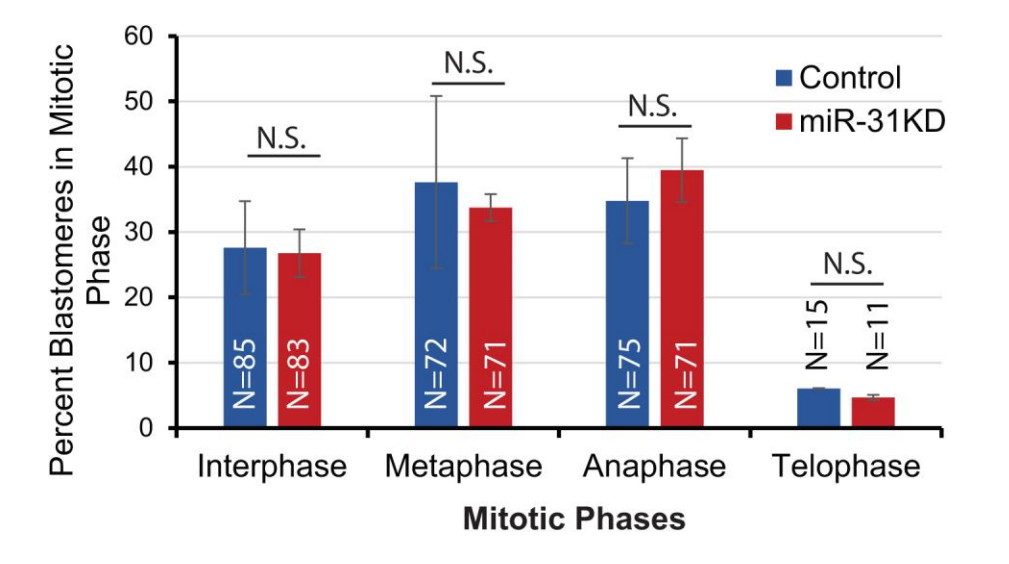


Fig. S1. miR-31 does not seem to regulate a particular phase of mitosis. Zygotes were injected with control (miR-124 LNA inhibitor) or miR-31 LNA inhibitor. The number of blastomeres in each mitotic phase was tabulated. No significant difference was observed between the control and miR-31 inhibited blastomeres. Cochran-Mantel-Haenszel statistical test was used to analyze four biological replicates; N.S. (P>0.05), not significant. N = number of blastomeres. Data are mean+s.e.m.

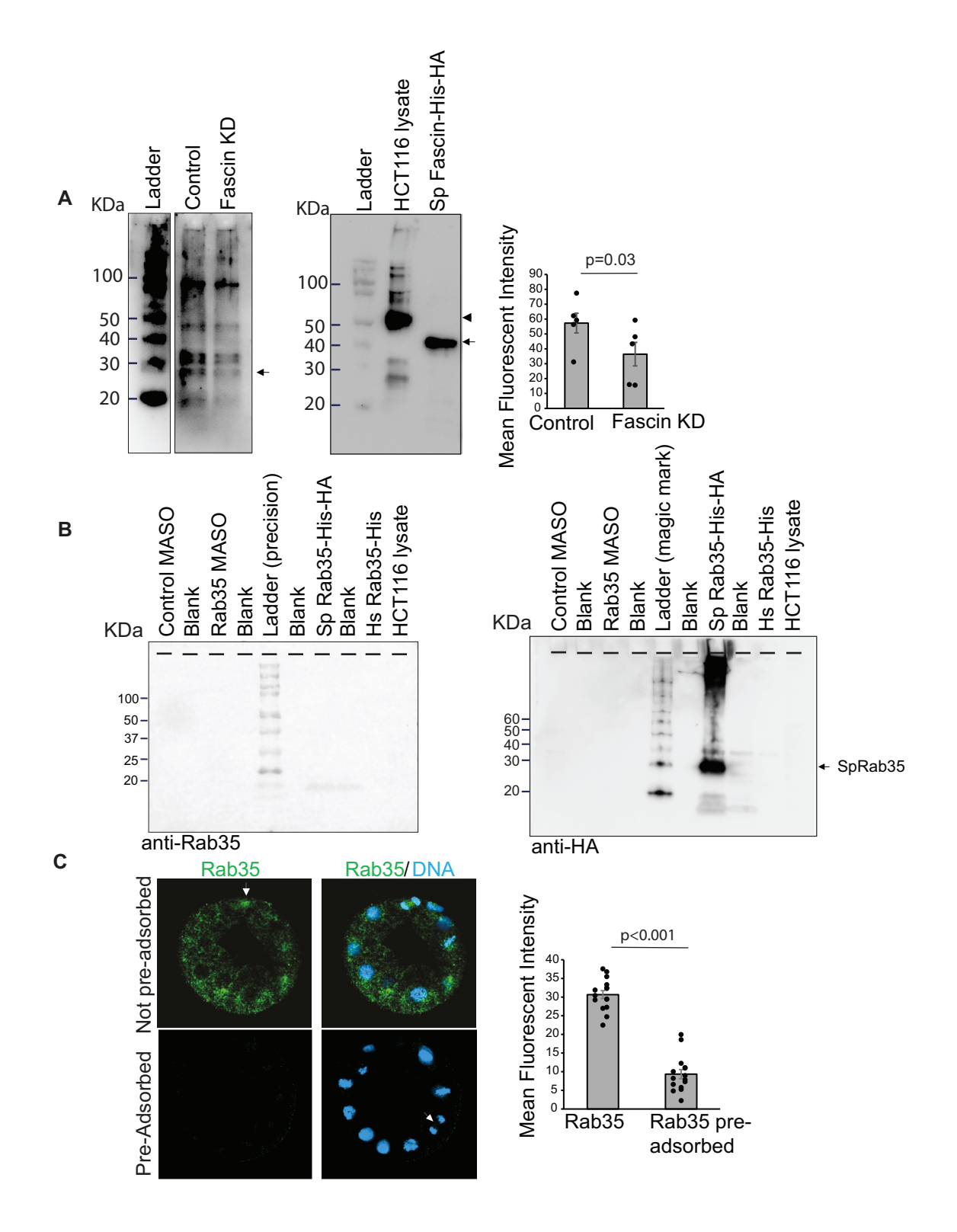


Fig. S2. Test specificity of Fascin and Rab35 antibodies.

(A) A representative western blot is shown with the Fascin antibody. We injected 150 newly fertilized eggs with control or Fascin MASO and collected 16-32 embryos for the western blot. The expected size of the sea urchin Fascin is 28KDa (arrow). Western blot is also conducted with lysates from HCT116 cells (arrow head, 55KDa) and bacteria expressing the recombinant sea urchin Fascin protein (arrow, 39KDa). The expected size of the recombinant sea urchin Fascin fused with 6xHIS and HA tag is 39KDa. Quantification of Fascin in five replicates of control and Fascin MASO-injected 32-cell stage embryos indicated a significant decrease of Fascin protein in Fascin MASO-injected embryos compared to the control injected embryos, indicating that the Fascin MASO is able to knockdown Fascin. Student t-test with p=0.03. (B) A western blot using the Rab35 antibody was conducted. The Rab35 antibody did not recognize the Rab35 protein in immunoblots (expected size at 23KDa for endogenous protein and 29KDa for recombinant Rab35 protein). Lysates tested include 150 of control and Rab35 MASO-injected embryos, bacterial lysate expressing sea urchin Rab35-HIS-HA, bacterial lysate expressing human Rab35-HIS recombinant protein (23.8KDa), and the HCT116 cells (23KDa), This blot was stripped and incubated with the HA antibody which recognized the bacterial lysate containing the recombinant sea urchin Rab35 protein (29KDa, arrow). The colorimetric Precision Plus Protein Standard ladder (left) and the Magic Mark ladder (right, visible via chemiluminescence) were loaded in the same lane. This result indicates that the Rab35 antibody did not work in a western immunoblot but works well in immunolabeling experiments. (C) We conducted preadsorption study to test the specificity of the Rab35 antibody. Rab35 antibodies were either preadsorbed with bacterial lysate expressing sea urchin recombinant Rab35 or vector alone. Results indicate that the level of Rab35 immunolabeling is significantly lower in embryos incubated with preadsorbed Rab35 antibody compared to the control, indicating that the Rab35 antibody recognizes the sea urchin Rab35. 15 embryos in 3 replicates were quantified. Note that the Rab35 enrichment at the mitotic spindle is not observed in preadsorbed Rab35 immunolabeling of anaphase blastomere (arrow head), indicating the specificity of Rab35 at the spindle. Student t-test with p<0.001.

Table S1. Proteomics analysis of miR-31 targets

	But the same	The difference of the means between control and treated samples in log2 1-C1										
Accession	Protein name	1-C1	1-C2	2-C3	2-C4	Overall	1-C1 Norm	1-C2 Norm	2-C3 Norm	12-C4 Norro	verall Nor	hold difference
VD 004470000 4	Positive significant and a state of the stat				0.45	2.20	1.68	3.28	0.38	0.47	2.22	4.6784
XP_001179300.1 XP_001179181.1	PREDICTED: similar to cyclophilin	0.86 1.21	7.04 0.95	0.61 1.43	1.14	2.36	1.08	0.79	1.09	0.47 1.30	2.23 1.12	2.1685
XP_001179181.1 XP_001177415.1	PREDICTED: similar to tubulin, alpha 2 isoform 2 PREDICTED: similar to HLC-32	1.12	1.01	0.58	0.23	1.21 0.73	0.62	0.79	0.05	0.62	0.61	1.5285
				0.58	0.23		-0.04		0.05	0.84	0.61	
XP_791790.1 XP_780390.1	PREDICTED: tubulin B-chain	0.26 1.64	0.24	1.56	1.17	0.38	0.53	0.25		1.86	1.06	1.1670 2.0796
XP_780390.1 XP_001176123.1	PREDICTED: similar to putative ribosomal protein S14e	0.13	0.85	1.04	1.17	0.59	0.53	1.14 0.62	0.70 0.98	0.94	0.46	1.3723
XP_001176123.1	PREDICTED: similar to gelsolin	0.13	0.93	0.43	0.48	0.59	0.16	0.62	0.98	0.94	0.46	1.3514
XP_791430.1 XP_001178269.1	PREDICTED: similar to Histone H2AV (H2A.F/Z) PREDICTED: similar to EBP-alpha	0.00	1.19	0.43	0.48		0.70	0.75	-0.05	0.05		1.6261
XP_001176269.1 XP_791056.2		0.62 0.97	1.19	0.07		0.86	0.78	0.75	-0.05		0.70	
XP_791056.2 XP_001189622.1	PREDICTED: hypothetical protein, partial	1.38	1.03	1.00	0.69 0.79	0.83		1.64	0.02	0.60	0.67 0.98	1.5864 1.9666
XP_001189622.1 XP_001181395.1	PREDICTED: similar to Acyl-Coenzyme A dehydrogenase, long chain	0.25	-0.05	1.08	1.53	1.06 1.10	1.24 -0.07	-0.17	0.93 1.24	0.83	0.98	1.9881
XP_001181395.1 XP_001177431.1	PREDICTED: similar to arginine kinase	0.25	-0.05		0.95		-0.07	-0.17		1.57 1.15	1.29	2.4482
_	PREDICTED: similar to tubulin, alpha 2 isoform 2	0.13	0.11	2.19	0.95	1.36	0.12	0.00	1.70 0.97			
NP_999721.1	histone H2b-2	0.13	0.11	0.92		0.50	-0.13	0.09		0.81	0.38	1.2990
XP_781777.1 XP_794336.1	PREDICTED: similar to Ribosomal protein S2	1.00	-0.08 0.87	0.72 0.19	0.60	0.47	0.78	-0.33 0.79	0.55	0.56	0.37	1.2931
XP_794336.1 XP_801793.1	PREDICTED: similar to creatine kinase, mitochondrial	1.00	0.87		0.10	0.63	0.78	0.79	0.04 1.03	1.04		1.4066
	PREDICTED: similar to ATP synthase, H+ transporting	-0.73		1.38	1.09	1.09	-0.87				1.03	2.0466
XP_001190124.1 XP_788276.1	PREDICTED: hypothetical protein	0.97	0.00		0.81	1.04 0.59	-0.87	0.00	1.44 0.31	0.72 0.37	0.83	1.7808 1.4113
XP_788276.1 XP_001178596.1	PREDICTED: similar to HS1 (14, 3,3 protein)		0.86	0.43	0.42		1.81	0.69	0.31	0.37	1.27	2.4078
XP_001178596.1 XP_782717.2	PREDICTED: similar to apolipophorin precursor protein	1.93	0.95	1.53	0.41	1.46 0.97	1.81	0.72	1.32	0.48	0.90	1.8677
	PREDICTED: similar to chaperonin containing TCP1, subunit 6A isofor		0.42				4.40	0.47			0.90	
NP_999808.1	heat shock protein gp96	1.56	0.42	0.34	0.32	0.43	1.42	0.17	0.06	0.46		1.2742
NP_999714.1	early histone H1	1.51	1.39			1.45	1.34	1.22			1.28	2.4351
XP_781507.1	PREDICTED: similar to ribosomal protein L12, partial	2.41	0.69			1.55	2.27	0.43	0.15	2.12	1.35	2.5516
XP_001188952.1	PREDICTED: similar to PRO1633, partial chapertone containing TCP1	0.10	0.01	0.30	0.38	0.31		0.15	0.17	0.40	0.26	1.1952
NP_999743.1	mitochondrial ATP synthase alpha subunit precursor	0.19	0.21	0.39	0.19	0.20	-0.07	0.15	0.10	0.29	0.09	1.0617
XP_780172.1	PREDICTED: similar to adenosylhomocysteinase	0.26	0.09	0.35	0.17	0.20	-0.10	0.17	0.12	0.23	0.09	1.0612
XP_001176458.1	PREDICTED: similar to elongation factor 1 alpha isoform 1	0.13	0.11	0.34	0.29	0.24	-0.06	0.03	0.31	0.20	0.12	1.0870
XP_001194483.1	PREDICTED: hypothetical protein, partial			1.13	0.95	0.97			1.60	0.20	0.89	1.8478
XP_782254.2	PREDICTED: similar to RACK	0.61	0.03	0.03	0.05	0.13	0.24	0.10	-0.10	0.08	0.02	1.0171
XP_795649.2	PREDICTED: similar to D-3-phosphoglycerate dehydrogenase	0.37	0.21	0.01	0.01	0.13	-0.15	0.39	-0.04	-0.04	0.02	1.0144
NP_999692.1	cytoskeletal actin Cylllb	0.74	-0.51			-0.34	0.39	-0.45			-0.55	0.6825
XP_001188929.1	PREDICTED: similar to malate dehydrogenase	1.17	4.00			1.17	1.03				1.03	2.0354
XP_001187263.1	PREDICTED: similar to glutathione reductase	1.15	1.02			1.09	1.01	0.77			0.89	1.8529
XP_783473.1	PREDICTED: hypothetical protein	-0.21	0.38	0.02	0.75	0.08	-0.30	0.16	-0.15	0.87	-0.06	0.9601
XP_001190324.1	PREDICTED: hypothetical protein	-0.80	-0.94	0.34	0.51	-0.03	-1.34	-0.80	0.18	0.55	-0.13	0.9167
XP_788858.1	PREDICTED: similar to MGC68486 protein, partial	-0.34	0.25	1.84	-0.91	-0.01	-0.55	0.14	1.46	-0.95	-0.14	0.9069
XP_783293.1	PREDICTED: similar to H(+)-transporting ATPase beta subunit	0.28	0.26	0.04	0.06	0.12	0.09	0.13	-0.06	0.02	0.01	1.0098
XP_780116.2	PREDICTED: similar to glyceraldehydephosphate dehydrogenase isofo	0.15	0.03	0.38	0.07	0.09	-0.03	-0.08	-0.07	0.21	-0.03	0.9767
XP_001196788.1	PREDICTED: similar to glutamine synthetase	-0.45	-0.39	1.29	0.55	0.07	-1.00	-0.13	0.66	0.91	-0.04	0.9714
XP_797562.1	PREDICTED: similar to ENSANGP0000011796			0.59	0.58	0.59			0.53	0.54	0.53	1.4462
XP_001177774.1	PREDICTED: similar to RAB35, member RAS oncogene family	1.79	2.12			1.95	1.65	1.87			1.76	3.3792
XP_783048.1	PREDICTED: similar to Slc25a3-prov protein	0.92	1.34			1.13	0.77	1.09			0.93	1.9062
XP_001177664.1	PREDICTED: similar to Peptidase (mitochondrial processing) beta isof	1.06	0.44			0.75	0.91	0.19			0.55	1.4680
XP_001184576.1	PREDICTED: similar to Grp58-prov protein	-0.03	1.25	0.30	-0.49	0.21	-0.31	1.16	0.10	-0.50	0.07	1.0531
XP_001176440.1	PREDICTED: similar to thioredoxin peroxidase	0.28	0.53	0.54	0.59	0.46	0.26	0.22	0.71	0.29	0.33	1.2592
XP_784254.1	PREDICTED: similar to Ribosomal protein S11	0.34	0.22			0.28	0.17	0.05			0.11	1.0814
XP_001191897.1	PREDICTED: similar to hyalin			0.88		0.88			0.50		0.50	1.4151
XP_780884.1	PREDICTED: similar to H4 histone protein		l	0.31	0.40	0.36	1	<u> </u>	1.07	-0.35	0.30	1.2275
	T											
Annotation:	1-C1: 51/C1&52/C1 Vs C1/C1&C2/C1											
	1-C2: S1/C2& S2/C2 Vs C1/C2&C2/C2											
	2-C3: S3/C3&S4/C3 Vs C3/C3& C4/C3											
	2-C4: S3/C4&S4/C4 Vs C3/C4& C4/C4											
	Overall: S1/C1&S2/C1&S1/C2&S2/C2&S3/C4& S4/C4&S3/C3&S4/C3 V	/s C1/C1&0	2/C1&C1/	C2&C2/C2	&C3/C3&C	4/C3&C3/C	4& C4/C4					
	Positive significance (Control < Treated sample)											

Table S2. RNA pulldown (miR-31 mimic vs. control)

Row.names	SPU_COMMON_NAME	SPU_ID	GENEBANK_HIT	logFC	logCPM	LR	PValue	FDR	S13.cpm	S14.cpm	S15.cpm						S21.cpm	S23.cpm	S25.cpm	\$26.cpm !	S27.cpm	S13.count 9	14.count S15	.count S16	.count S17.cou	nt S18.count	S19.count	S20.count	S21.count	S23.count S2	25.count S	26.count 9	27.count
WHL22.673644	Sp-II1r/Rs1(d)	SPU_000409	none	4.97986		44.9094	2.06E-11				0.43291			0.98192			22.4813	3.09937			1.36434	33	178	3	57 9	7	5	1	234	22	6	8	12
WHL22.546681		SPU_025378	CERAC1H	3.60793		38.9727		5.09E-06			2.16456					0.72678		1.54968			5.00257	84	550	15	112 5	7 11		5	172	11	23	32	44
WHL22.434852		SPU_023199		2.1581	9.88795	36.4608	1.56E-09	1.23E-05			291.494		1757.61			417.317					503.327	3008			8780 1445		1355	2871	17874	3783	4657	4123	4427
WHL22.720032	Sp-II1r/Rs1	SPU_013950		4.62981	4.5526		2.13E-08	0.00013			1.73165			1.12219	5.56975	0.58142		11.1295			13.7571	116	511	12	229 38	2 8	39	4	690	79	67	40	121
WHL22.331472	NA	NA	NA	4.9916	1.28995			0.00014			0.43291			0.14027	0	0.14536			0.60058	1.12583	0.90956	10	36	3	51 4	5 1	0	1	39	1	5	10	8
WHL22.546687	SPU_016346	NA	NA	3.17481	4.71272	29.4087	5.86E-08	0.00023	107.6	64.7842	5.91647	62.509	21.6433	11.2219	9.99699	1.59891	25.5556	17.1874	7.8075	9.7947	14.894	177	638	41	349 17	80	70	11	266	122	65	87	131
WHL22.433537	Sp-Kirrel2L_6	SPU_003193	NP_954649.2	4.25102		28.4646	9.54E-08	0.00032	16.4136		0.57722		8.02506	0	0	0.29071	3.74688	0.14088	1.5615		0.56847	27	222	4	52 6	5 0	0	2	39	1	13	16	5
WHL22.434849	Sp-Fscn1		NP_999701.1	3.19949	6.20995	25.4864	4.46E-07	0.00132	126.446	489.537	13.5646	48.3594	140.317	21.3216	4.99849		162.365		7.92761	12.0464	5.79844	208	4821	94	270 115	152	35	18	1690	172	66	107	51
WHL22.350265	Sp-Actb_2	SPU_015278	NP_001092.1	4.97421				0.00137		8.83421		12.1794	12.2808	0.14027			9.31916		3.00288	4.72848	1.81912	9	87	0	68 10	1 1	11	2	97	6	25	42	16
WHL22.512518	Sp-Cyld_1	SPU_011766	BAG51293.1	3.01935				0.00137			3.17469		52.1629			4.9421					62.8733	123	881	22	319 42		137	34	664	137	505	381	553
WHL22.620148	Sp-MeprinAaL	SPU_030013		2.66257	10.8125	23.7076	1.12E-06	0.00242			673.323			376.355		189.544	4005.32	565.071	645.74	267.497	1004.27	8556	64361	4666	4846 2011	2683	2768	1304	41690	4011	5376	2376	8833
WHL22.461785	Sp-Abcc10a	SPU_004692	NM_033450	2.76413		21.8881	2.89E-06	0.00571	43.1617	63.6672	4.18482			13.4663		1.01749			4.08392		7.27647	71	627	29	125 34	96	20	7	118	16	34	32	64
WHL22.80947	SPU_025752	NA	NA	4.81088	0.77844	21.252	4.03E-06	0.00734	6.07911	3.04628		3.58218	2.67502			0.14536			0.36035		0.22739	10	30	0	20 2	2 1	3	1	43	2	3	6	2
WHL22.589997	Sp-Hypp_412	SPU_004329	EDO47093.1	3.88476	1.58909	20.8412	4.99E-06	0.00739	2.43164	4.56942	0.72152	11.1047	2.79661	1.12219	1.14251	0.14536	4.13117	1.69056	0.72069	3.71523	2.04651	4	45	5	62 2	3 8	8	1	43	12	6	33	18
WHL22.20686	SPU_005155	NA	NA	3.52045	3.27591	21.063	4.44E-06	0.00739	34.6509	39.1955	1.01013	2.32841	6.32277	2.52493	0.28563	0.29071	23.3459	16.6239	0.48046	4.95364	1.36434	57	386	7	13 5	2 18	2	2	243	118	4	44	12
WHL22.577814	NA	NA	NA	2.75789	10.3734			0.00739	3393.36		537.677	2162.2	2219.66		270.347	104.511		419.26	659.553		920.474	5582	41397	3726	2072 1825	1957	1893	719	30167	2976	5491	2187	8096
WHL22.650386	NA	NA	NA	3.21651	4.76945	20.5044	5.95E-06	0.0082	88.1471	94.3331	3.6076	53.1953	11.1864	20.9008	11.1395	2.03498		28.5987	4.80461	5.51656	20.9199	145	929	25	297 9	149	78	14	292	203	40	49	184
WHL22.630932	NA	NA	NA	2.45636	4.02572	20.4153	6.23E-06	0.0082	50.4566		5.48355		32.5866		4.85568	4.06996	22.9616	9.2981	6.00577	3.9404	10.5736	83	405	38	162 26		34	28	239	66	50	35	93
WHL22.620148	Sp-MeprinAaL	SPU_030013		2.40732	10.7632		1.03E-05	0.01171	4315.56		807.958		2550.39			228.79	3887.53	588.739	626.281	291.027	1000.86	7099	65280		3978 2097	2875	2244	1574	40464	4179	5214	2585	8803
WHL22.433365	Sp-Mvp	SPU_000881	NP_001116989	2.16346		19.4397	1.04E-05	0.01171			113.712		579.02				518.606	318.812	303.291	247.007	286.056	574	5949		3848 476		921	710	5398	2263	2525	2194	2516
WHL22.433365	Sp-Mvp	SPU_000881	NP_001116989	2.15648	8.36802	19.5099	1.00E-05	0.01171	365.355					96.7889			520.047		303.291	245.881	285.033	601	6276	789	3824 475	690	915	711	5413	2246	2525	2184	2507
WHL22.620148	Sp-MeprinAaL	SPU_030013		2.73726	10.3296	19.1414	1.21E-05	0.01198			491.932		1754.33			95.3534	2995.58	422.641	508.088	207.152	691.151	6578	44390	3409	9635 1442	1896	1426	656	31180	3000	4230	1840	6079
WHL22.620148	Sp-MeprinAaL	SPU_030013		2.56685	10.724	19.2533	1.14E-05	0.01198	4745.96	6651.35	718.49	2255.7	2159.47	365.974	260.636	169.776	4028.28	551.828	548.807	267.497	839.75	7807	65503	4979	2594 1776	2609	1825	1168	41929	3917	4569	2376	7386
WHL22.620148	Sp-MeprinAaL	SPU_030013		2.50969	10.5428	19.1689	1.20E-05	0.01198	3855.37	5617.34	675.92	2139.63	2004.2	331.607	254.923	165.996	3554.44	516.749	528.748	257.252	819.626	6342	55320	4684	1946 1648	3 2364	1785	1142	36997	3668	4402	2285	7209
WHL22.563609	Sp-Mdh	SPU_003445.:	1 NA	-3.43016	1.79906	18.7459	1.49E-05	0.01415	3.64747	1.32005	7.50381	0	0.72955	3.08602	2.57065	8.72135	1.05681	2.53585	4.44427	2.81457	2.72868	6	13	52	0	5 22	18	60	11	18	37	25	24
WHL22.350285	Sp-Act_1	SPU_021545	AAA30034.1	2.60352	2.6084	18.3217	1.87E-05	0.017	13.982	10.3573	0.72152	7.34346	4.98526	1.40274	1.85658	2.61641	18.6383	5.49433	4.08392	4.39073	3.06976	23	102	5	41 4	1 10	13	18	194	39	34	39	27
WHL22.765708	Sp-FtzF	SPU_013843	NA	4.38079	2.05649	17.7784	2.48E-05	0.02178	4.25538	6.1941	0.28861	21.6722	0.72955	0.28055	2.14221	0.58142	5.95658	0.42264	1.08104	0.33775	7.73125	7	61	2	121	5 2	15	4	62	3	9	3	68
WHL22.471859	Sp-Hypp_1984	SPU_011507	AAO51215.1	2.92948	5.36266	17.4145	3.01E-05	0.02455	119.151	139.012	4.76203	69.6733	14.591	22.4438	18.1374	5.52352	54.3778	56.0704	10.3299	8.78146	33.1989	196	1369	33	389 12	160	127	38	566	398	86	78	292
WHL22.21036	Sp-Nr1m3	SPU_013178		1.92777	6.71419	17.4542	2.94E-05	0.02455	219.456	263.3	32.3241	226.394	155.151	20.1994	57.9825	72.6779	172.741	57.62	49.968	20.6027	70.2634	361	2593	224	1264 127	5 144	406	500	1798	409	416	183	618
WHL22.765708	Sp-FtzF	NA	NA	4.27472	1.98053	17.2822	3.22E-05	0.02544	4.25538	5.4833	0.28861	20.2393	0.72955	0.28055	2.14221	0.58142	5.38013	0.42264	1.08104	0.33775	7.61756	7	54	2	113	5 2	15	4	56	3	9	3	67
WHL22.184359	Sp-Cplcallb	SPU_009483	47551035	1.48433	10.9011	17.0174	3.70E-05	0.0283	6028.66	4275.45	871.452	1875.45	2288.84	1069.45	700.503	819.226	3357.2	1947.25	889.214	1091.27	697.859	9917	42105	6039	.0471 1882	7624	4905	5636	34944	13822	7403	9693	6138
WHL22.286588	Sp-Dusp16	SPU_003347	XP_787378.2	1.66907	6.79064	16.9016	3.94E-05	0.02851	156.841	240.656	38.6735	190.034	265.435	45.589	41.4161	64.538	140.844	83.8238	79.2761	64.1722	78.5632	258	2370	268	1061 218	3 325	290	444	1466	595	660	570	691
WHL22.286588	Sp-Dusp16	NA	NA	1.6343	6.85403	16.8283	4.09E-05	0.02851	174.471	271.119	40.2608	190.393	269.204	46.1501	41.7017	68.8987	149.299	85.3735	80.7175	64.8477	77.9947	287	2670	279	1063 221	4 329	292	474	1554	606	672	576	686
WHL22.184359	Sp-Cplcallb	SPU_009483	47551035	1.47735	10.6492	16.8627	4.02E-05	0.02851	5261.47	3498.55	723.108	1620.4	1948.39	870.399	607.674	723.291	2723.88	1595.61	733.785	878.258	581.663	8655	34454	5011	9047 1602	4 6205	4255	4976	28352	11326	6109	7801	5116
WHL22.626091	Sp-Gat_2	SPU_000076	AAF70819.1	2.70953	3.02471	16.6143	4.58E-05	0.03047	2.43164	1.4216	8.08103	32.0605	50.947	4.76931	3.99879	0.14536	0.96074	0.14088	0.96092	2.13907	2.2739	4	14	56	179 41	9 34	28	1	10	1	8	19	20
WHL22.620148	Sp-MeprinAaL	SPU_030013		2.70779	10.715	16.5937	4.63E-05	0.03047	5035.94	6408.86	684.29	2125.66	2225.5	355.594	235.929	104.947	4090.92	541.121	583.52	255.563	785.29	8284	63115	4742	1868 1830	3 2535	1652	722	42581	3841	4858	2270	6907
WHL22.626091	Sp-Gat_2	SPU_000076	AAF70819.1	2.66506	3.05815	16.5246	4.80E-05	0.03079	2.43164	1.72622	8.36963	32.7769	52.4061	4.76931	3.99879	0.14536	0.96074	0.14088	0.96092	2.25166	2.1602	4	17	58	183 43	1 34	28	1	10	1	8	20	19
WHL22.521303	Sp-Hypp_772	SPU_015150	XP_958002.1	-1.50793	6.41352	15.5771	7.92E-05	0.04938	39.5142	68.3382	66.5242	34.0307	25.0479	35.349	71.9783	192.742	60.1422	119.889	130.085	62.0331	141.777	65	673	461	190 20	5 252	504	1326	626	851	1083	551	1247

Table S3. LNAs and morpholinos used in this study

	Sequence (5'-3')
hsa-miR-31-3p miRCURY LNA miRNA	AGGCAAGAUGUUGGCAUAGCU
Mimic-biotinylated	
miR-31 LNA power inhibitor	UGCUAUGCCAACAUAUUGCCAU
miRCURY LNA miRNA Inhibitor Control	TAACACGTCTATACGCCCA
Control miR-124 LNA power inhibitor	GCATTCACCGCGTGCCTTA
miR-31 LNA in situ detection probe	TGCTATGCCAACATATTGCCAT
Scrambled LNA in situ detection probe	GTGTAACACGTCTATACGCCCA
Fascin translational MASO	ATCAACATATTTCACAATGCCTGCT
Negative control MASO (Hs β-globin)	CCTCTTACCTCAGTTACAATTTATA
Fascin TP	GAACAGACAAGAGTGCAATGTGACA
Rab35 TP	AGAATGGCAAAAAACGTAAAGAGT

Table S4. Primers used for cloning in this study

	Forward (5' to 3')	Reverse (5' to 3')
	Primers for cloning <i>in situ</i> probes	(Sp6 sequence is underlined)
Sea urchin <i>Fascin</i>	GATGGGGATTCGGTAGGTTT	ATTTAGGTGACACTATAGTTCTTAGACGCTGGGACCTG
Sea urchin Rab35	ATGGCGAGGGAATACGATCA	TATTTAGGTGACACTATAGTCATTTACCGCAGCATTTTC
Sea urchin <i>β-actin</i>	TGTCTTCCCATCTGTTGTCG	<u>ATTTAGGTGACACTATAG</u> TCTTCATGGAGGGTGGAGTC
Sea urchin Gelsolin	CGGATCGTCAAGGT	<u>ATTTAGGTGACACTATAG</u> GGCAACCAAGGTGTCTCAGT
Mammalian <i>Fascin</i>	GGAGAGCAGGTGGCAATCTT	<u>ATTTAGGTGACACTATAG</u> CCGACCTCCTTTGTTCAGCA
Priı	mers for cloning into <i>Renilla luciferase</i> and muta	genesis (restriction enzyme sites underlined)
Fascin	TGCCCTCGAGACAAATTGGGCTTGAAAGAAG	TGCGGCCGCTTTCTAATGACGGCGTGCAT
Fascin seed 1 mut	GTTCAGTGCTTCTGGTATGTAGGAGTTGTCACGGACACTGG	CCAGTGTCCGTGACACTCCTACATACCAGAAGCACTGAAC
Fascin seed 2 mut	GTATGTTCCATTATCAACAGAACAGATAGGAGTGCAATGTGAC AATAAAAAAGTA	TACTTTTTTTTTTTCACATTGCACTCCTATCTGTTCTGT
Rab35	CTCGAGTACCGCTCCCTTATGCTAGTGGAC	<u>GCGGCCGC</u> TCTTGTTACAATGACAAAACAAAAG
Rab35 mut	TCGACACAGAATGGTAGAAAAACGTAAAGAGTATGATAGGGGCG	CGCCCCTATCATACTCTTTACGTTTTTCTACCATTCTGTGTCGA
Gelsolin	GA <u>CTGCAG</u> AGCTTTTAGCAACCAAGACGA	GA <u>GGTACC</u> GGGCAACACTGCATTTGGG
Gelsolin mut	CACTGGTCGTTCATGTCAGGTACGACTGATTTTTAAGTGCATG	CATGCACTTAAAAATCAGTCGTACCTGACATGAACGACCAGTG
β-actin	<u>GGTACC</u> ATGTGTGACGACGATGTTGC	<u>GCGGCCGC</u> TTAGAAGCACTTCCTGTGGA
β-actin seed 1 mut	ACCGACAACAGATGGTAATACAGCTCGTGGTGCATCG	CGATGCACCACGAGCTGTATTACCATCTGTTGTCGGT
β-actin seed 2 mut	CAAGACGAAGAATGGAATTAGGGAGGGCGTACCCTTCA	TGAAGGGTACGCCCTCCCTAATTCCATTCTTCGTCTTG
β-actin seed 4 mut	GTGGCCGAGGACATACGGTTGGAAGAGGGCTTCGG	CCGAAGCCCTCTTCCAACCGTATGTCCTCGGCCAC